ABSTRACT

AL-DAWOOD, KHALDOON ALI. Modeling, Simulation and Optimization of Lead-Cooled Fast Reactors. (Under the direction of Scott Palmtag.)

The last two decades witnessed an increasing interest in Liquid Metal-cooled Fast Reactor (LMFR) technology. This was associated with the establishment of the Generation IV International Forum (GIF) in 2001. Sodium-cooled Fast Reactors (SFRs) have traditionally received the majority of the attention. Lead-Cooled Fast Reactor (LFR) technology has recently gained more momentum in research and development. This is due to the neutronic, chemical and thermal advantages that lead coolant has that potentially enables safer and more economical plant designs.

The computer code `LUPINE` has been developed at North Carolina State University for the modeling and simulation of LMFRs. The code performs coupled neutronics, thermal hydraulics and thermal expansion calculations. In the first part of this thesis, the capabilities of `LUPINE` have been extended to enable the modeling and simulation of LFRs. These capabilities include the neutronic and thermal models of lead coolant, gap region model and thermal models of uranium mononitride (UN) fuel. The theory of implementing these capabilities in `LUPINE` has been presented.

The second part of this research investigates the optimization of LMFR designs. To do this, a new general purpose Design and Optimization Methodology (DOM) has been developed. The theory behind this methodology is presented and a Python program was developed to automate the application. The method was applied to the Westinghouse Electric Company LLC (WEC) long-life core LFR with the goal of coming up with a better economically performing core. An optimized core was developed that decreased the Levelized Cost Of Electricity (LCOE) by 2.56 [%], which is a cost savings of 17,765,685 [$] over the life of the plant.

Modeling, Simulation and Optimization of Lead-Cooled Fast Reactors

by
Khaldoon Ali Al-Dawood

A thesis submitted to the Graduate Faculty of
North Carolina State University
in partial fulfillment of the
requirements for the Degree of
Master of Science

Nuclear Engineering

Raleigh, North Carolina

2021

APPROVED BY:

Yousry Azmy

David Kropaczek

Scott Palmtag
Chair of Advisory Committee

DEDICATION

I am dedicating this work to my lovely family.

BIOGRAPHY

Khaldoon Al-Dawood was born in Irbid, Jordan. He attended private and public schools for his primary education. Dawood attended Al-Ramtha school for his high school. He earned a Bachelor's degree from Jordan University of Science and Technology in Nuclear Engineering. After the Master's degree, Dawood will remain at NC State to pursue a Ph.D. in Nuclear Engineering.

ACKNOWLEDGEMENTS

I would like to take this opportunity to express my deep sense of thanks and gratitude for those who have had a direct impact on this journey.

I am extremely grateful to my parents Ali and Sana', and my siblings for believing in me and providing the necessary support. I would like to express my deepest appreciation to my advisor Dr. Scott Palmtag for his guidance and support. His vision, insight and dedication have always inspired me.

I also would like to thank my friends Majdi, Vincent, Mayzan, Sara, Drishya, William, Simone, Johnny, Thamer, Brian, Rofhiwa, Chase, Divshi, Fatma, Zainab, Faris and Majd. Thank you all for being with me at all times and for making life intellectually and socially exciting.

TABLE OF CONTENTS

LIST OF TABLES

LIST OF FIGURES

CHAPTER

1

INTRODUCTION

1.1 Motivation

In light of the recent interest in modeling and simulation of advanced reactors generally, and Liquid Metal-cooled Fast Reactors (LMFRs) specifically, the LMFR Utility for Physics Informed Nuclear Engineering `LUPINE` computer code has been developed [DP21]. The code solves the Simplified P_N (SP_N) multigroup neutron transport equation using the Finite Element Method (FEM). It incorporates a thermal hydraulics and a thermal expansion model allowing multiphysics simulation. During the initial development of `LUPINE`, the code was built and tested for the modeling and simulation of Sodium-cooled Fast Reactors (SFRs) with U10Zr metallic fuel [Daw19]. In this work, `LUPINE` modeling and simulation capabilities were extended to model Lead-Cooled Fast Reactors (LFRs). The new capabilities include lead coolant thermal properties, lead neutronic model, nitride fuel model, gas gap region model, and the mass flow distribution control.

Optimizing reactor core design is important for the effective utilization of nuclear fuel resources. It is also crucial for enhancing the economic performance and improving the safety of the design. LMFR cores optimization has been investigated in very few literature. In this thesis, a LMFR core design and optimization methodology is proposed. The methodology is based on the effective sampling of the design space and the elimination of regions in the search space with invalid reactor designs. A Python program was written to apply the methodology. A LFR design has been selected from the literature and the methodology was applied to it with the ultimate goal of optimizing the core to achieve better economic performance. A reduction of 2.56 [%] on the Levelized Cost Of Electricity (LCOE) was achieved.

1.2 Generation IV International Forum

In the beginning of the 21st century, the Generation IV International Forum (GIF) was established to focus the effort of the member countries on the development of the research necessary to test the feasibility and performance of fourth generation nuclear systems [Gen]. Based on this, GIF selected six technologies for further research activities. These technologies are Gas-Cooled Fast Reactor (GFR), LFR, Molten Salt Reactor (MSR), Supercritical Water-cooled Reactor (SCWR), SFR and Very High Temperature Reactor (VHTR). The definition of GIF proposed technologies was based on the goals shown in Fig. 1.1.

Figure 1.1 GIF Goals [Gen].

LMFRs are considered an attractive option for power production due to inherent safety features, better uranium utilization through conversion and breeding, improved actinide consumption, and improved thermal efficiency [YO19]. The benefits of metallic coolants are high thermal conductivity and the ability to operate the plant at nearly atmospheric pressure. The metallic coolant can operate at higher temperatures than water coolant, which can increase plant efficiency with higher steam temperature on the turbine island [Roe19]. This can, potentially, be reflected on the economic competitiveness of the technology. In this chapter, the effectiveness of LFR technology and the advantages it offers will be discussed. Also, the motivation for optimizing LMFRs generally and LFRs

specifically will be presented.

1.3 Lead Cooled Fast Reactors

In comparison to water coolant, liquid metal coolants are characterized by high thermal conductivity, lower heat capacity and smaller kinematic viscosity. This can be used to achieve better safety behavior of LMFRs compared to Light Water Reactors (LWRs) and higher plant efficiency. Compared to sodium coolant in SFRs, lead coolant is chemically stable with water and air, and has a higher boiling temperature (i.e. 2021 [K] [Sob11]). Lead features smaller elastic scattering energy loss compared to sodium. Thus, lead coolant provides smaller neutron moderation effect, allowing for a harder neutron spectrum. This also allows for increased coolant flow area in the fuel assembly without compromising neutron economy. The increased flow area reduces the axial pressure drop across the core and reduces the risk of core blockage [Pio16].

The chemical inertness of lead simplifies the design of the power plant by eliminating the need for an intermediate cooling system, which is used to isolate the nuclear island from the turbine island in SFRs. The high boiling temperature of lead alleviates the safety concerns with respect to coolant boiling. Additionally, since the primary coolant system is operated at atmospheric pressure, and possibly in pool mode, the need for a heavy pressure vessel and the complex systems needed to maintain the pressure level in the core, as is the case in LWR, is eliminated. The operation at atmospheric pressure also, potentially, eliminates the Loss Of Coolant Accident (LOCA) resulting in a simplification in safety provisions. Taking these into account, utilizing lead coolant can potentially lead to safer and more economical operation in addition to the gain in core design simplification. This makes LFRs worthy of investigating for the potential increased economic performance.

Lead coolant does have some drawbacks. For example, lead is more corrosive to the steel structural material compared to sodium. Several technologies have been proposed to mitigate the liquid metal corrosion. These include oxygen level control, metallic corrosion inhibitors and coating of structural materials [Zha13]. The oxygen level control technology has been demonstrated to be effective up to coolant temperatures of 820 [K] [Tuc06]. The technology has been utilized in the Russian Alpha-class submarine. Another disadvantage of the coolant is the erosive nature of lead to the oxide protective layer. This can be solved by reducing the coolant speed in the channel which, in turn, limits the cooling channel mass flow rate. Furthermore, lead has a high melting temperature, which raises concerns of coolant freezing. In-core heaters are proposed to solve this problem.

Historically speaking, the world has developed a significant experience with LFRs. In Russia, design of fast reactors cooled by lead or lead-alloys has been conducted since the 1960s [Ale14] (in the Soviet Union era). Such reactors have been designed and utilized in submarine propulsion in the period from 1960s-1990s. After the dissolution of the Soviet Union, the Russian Federation continued the Research and Development (R&D) in lead and lead alloy cooled fast reactors. The most recent in their R&D is the development of the BREST-OD-300 which is a lead-cooled medium sized power plant with an electric output of 300 [MWe]. This reactor has recently obtained its construction

license [Bre].

In western Europe, there is also a significant experience gained with LFRs. Several LFR designs have been developed. The most recent efforts started with the European Lead-Cooled SYstem (ELSY) project [Ale11]. The R&D efforts in this project led to the development of the Lead-cooled European Advanced Demonstration Reactor (LEADER) project which focused on industrial size critical reactors. The LEADER project led to the development of the Advanced Lead-cooled Fast Reactor European Demonstrator (ALFRED) which has an electric output of 120 [MWe] [Gra14].

In Asia, significant research experience has been gained in Japan, South Korea and China. Several LFR designs have been suggested. The Japanese Constant Axial shape of Neutron flux, nuclide density and power shape During Life of Energy production (CANDLE) design was suggested by Tokyo Institute of Technology [Sek01]. The core was initially designed to be cooled by sodium, but also allows for lead coolant. In South Korea, Proliferation-resistant, Environmental-friendly, Accident-tolerant, Continuable, and Economical Reactor (PEACER) has been suggested [Hwa07]. Finally, China is pursuing the development of an LFR through the China LEAd-based Reactor (CLEAR) project [Wu16].

In the United States of America (USA), the work on LFR technology started in 1997. More recently, the Small Secure Transportable Autonomous Reactor (SSTAR) has been suggested [Sie08]. The concept is one of the reference designs of the GIF-LFR Provisional System Steering Committee (PSSC). Most recently, a commercial version of an LFR has been suggested. This is the Westinghouse Electric Company LLC (WEC) long-life core LFR [Kim19]. It is a 950 [MW_{th}] reactor fueled with uranium mononitride (UN). This reactor has been adopted as the case study in this project. A detailed description of it will be presented in the chapters ahead. A summary of the worlds experience with LFR technology is presented in Table 1.1.

For decades of experience with nuclear power, uranium oxide and metallic fuels have been the only fuels used in fast power plants. In recent years, alternative fuels have been proposed. These include nitride, carbide and silicide fuels. Of special interest is the nitride fuel which has a higher thermal conductivity than the oxide fuel but maintains a similar melting temperature. Nitride fuel will be discussed in more details in Chapter 2.

Table 1.1 Summary of the worlds experience in LFRs

Reactor	Country	Power	Fuel	References
BREST-OD-300	Russia	700 MW_{th}	U-PuUN	[Bre] [Ada21]
ALFRED	Europe	300 MW_{th}	Mixed Oxide Fuel (MOX)	[Gra14]
CANDLE	Japan	200 MW_{th}	UN	[Sek01] [SY08]
PEACER	South Korea	850 MW_{th}	Metallic fuel	[Hwa07]
CLEAR	China	Research Reactor	UO_2	[Wu16]
SSTAR	USA	450 MW_{th}	Transuranic Nitride	[Sie08]
WEC long-life LFR	USA	950 MW_{th}	UN	[Kim19]

1.4 LMFR Design and Optimization

The design of LMFRs must account for four inter-dependent design phenomena. These are neutronics, thermal hydraulics, structural mechanics and economics. A reactor core design process can be summarized in three steps. First, the reactor objectives, core materials and design constraints are identified. The second is conceptualizing a reactor preliminary design based on the designer's experience associated with iterating over the design phenomena. If the reactor is to be optimized, a third step will be to identify the optimization algorithm and search space, and use the design constraints to come up with a better design compared to the original design by further iterating over the design phenomena aiming to achieve an improvement on the original design. The process is summarized in Fig. 1.2.

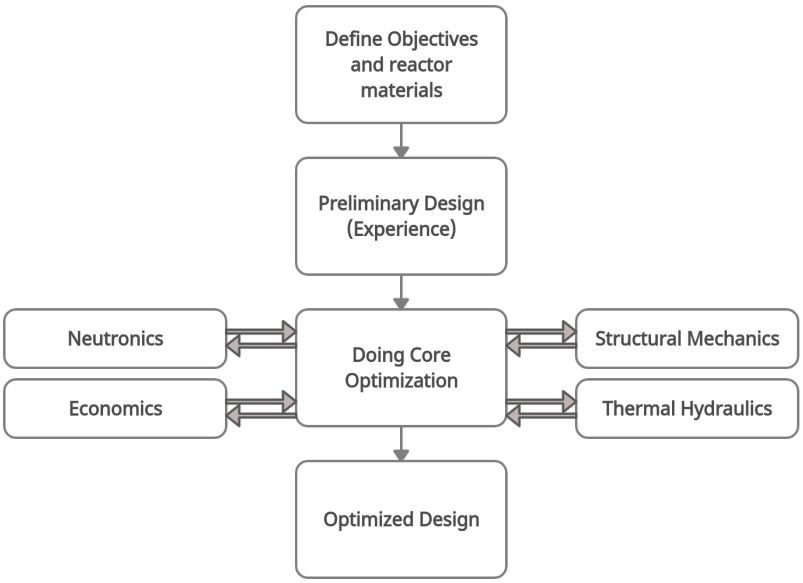

Figure 1.2 Reactor core design process [QG14]

Worth mentioning here is that liquid metals in LMFRs act as a coolant and not as a moderator. Additionally, the axial variation of coolant density in LMFR is small compared to that of water in LWRs. Thus, the coupling between neutronic and thermal hydraulics in LMFRs is weak. This makes the process of designing them easier since the configuration of a reliable design is easier to attain.

Since LMFRs are in their early stage of development for commercial market, the optimization work is focused on the development of reactor core Beginning Of Cycle (BOC) configuration that features efficient nuclear fuel utilization, and complies with safety requirements and design constraints.

In the nuclear industry, there are two styles of the optimization problem related to reactor core

design, namely; core optimization and fuel assembly optimization. The traditional goal is to achieve improved safety and economic performance while adhering to reactor design constraints. In the literature of nuclear reactor core design, the optimization problem has been mostly associated with core loading pattern design in both Pressurized Water Reactors (PWRs) and Boiling Water Reactors (BWRs). The fuel assembly design is an additional problem mainly associated with BWR fuel assembly design. Several optimization algorithms have been utilized to address the two styles of optimization problems. For example, in [KT91] the authors used Simulated Annealing (SA) algorithm to optimize a PWR core loading pattern. In [Fra03], Tabu search has been utilized to optimize the radial enrichment and gadolinia distribution of a BWR fuel assembly. Other algorithms, such as Genetic Algorithm (GA) and Particle Swarm Optimization (PSO) [DF95] [Bab09], and many other algorithms have been used for the same purpose.

In the literature, the efforts to optimize LMFRs, generally, and LFRs, specifically, can be found in two major works. The first and earlier is the development of the Assembly Design and OPTimization (ADOPT) code [QG14]. The code consists of twenty modules that model the neutronic, thermal hydraulic and structural mechanics of a fuel assembly. ADOPT has a built-in material properties library which allows for the modeling of a wide variety of materials used in LMFRs. The code was built to design and optimize Breed and Burn (B&B) reactors. However, the authors claim that the code can be used as a general-purpose LMFR assembly design. The code considers a set of design objectives and tries to perform neutronic analysis that aims to find the fuel volume fractions that achieves them. After that, the code iterates between the different physics modules to find fuel assembly design that achieves the desired fuel volumetric fractions while complying with thermal hydraulic and structural mechanics requirements and constraints. The code features fast convergence in optimizing reactors with high conversion ratio (i.e. B&B). However, the process of designing burner reactors is not as straightforward.

The second LMFR optimization attempt is the COre Design and OPTimization (CODOPT) code [Luo20]. The code replaces the iterative process in the core design process. It aims to find an optimum core design based on multiphysics analysis results and imposing constraints for intended core design. CODOPT iterates between three modules. These are neutronics, thermal hydraulics and geometry modules. The codes coupling between the neutronics and thermal hydraulics only considers the variation of material temperature. It neglects the effect of temperature on material densities as a result of thermal expansion. The thermal hydraulics analysis is utilized to study and analyze the hottest channel in the core. The code was used to optimize the Medium-power Modular Lead-cooled Fast Reactor (M^2LFR-1000)

In this thesis, the goal is to come up with a more general purpose design and optimization methodology. The methodology is based on an extended investigation of the search space. It uses a physics-informed elimination process to exclude regions of the search space where invalid designs exist. Then, by performing a multiphysics analysis, the optimal design in the search space is returned. In this work, the methodology will be tested on a LFR reactor core design. The work leverages from `LUPINE` multiphysics capabilities to accurately model LMFRs.

1.5 Thesis Organization

Chapter 2 will present the modeling and simulation capabilities added to LUPINE. These include the lead thermal properties, uranium mononitride properties, gas gap model and mass flow distribution control. Chapter 3 will detail the optimization methodology proposed in this project. In Chapter 4, modeling and simulation capabilities of LFR with nitride fuel are tested. The WEC long-life core LFR is presented and modeled using LUPINE. The coupled multiphysics simulation results are presented in addition to depletion results. Chapter 4 will also present the results of utilizing the optimization methodology in an attempt to optimize the economic performance of the WEC long-life core LFR core. Finally, conclusion and future work suggestions will presented in Chapter 5.

CHAPTER

2

MODELING AND SIMULATION OF LEAD FAST REACTORS USING LUPINE

2.1 LUPINE Background

LMFR Utility for Physics Informed Nuclear Engineering (LUPINE) is a multiphysics simulation suite for LMFRs [Daw19] [Pal21] [AD21]. The code solves coupled neutronics models with thermal hydraulics and thermal expansion models. The code can also perform depletion calculations enabling fuel cycle analysis. LUPINE enables the easy handling of reactivity coefficients calculation. This is achieved through the multi-statepoint input structure through which the user is able to control the solvers and state of reactor simulation. The FEM method enables performing a mesh refinement study without the need to regenerate the mesh.

The neutronics solver of LUPINE uses the FEM and employs a general, unstructured mesh to solve the SP_N multigroup neutron transport equations with an arbitrary truncation order N. Cross sections can be read from the LUPINE input file or from ISOTXS files created by MC^2-3 [LY13]. The neutronic models are coupled to the thermal hydraulics and thermal expansion models, and all the equations are solved simultaneously using a Picard iteration. The thermal hydraulic models include a radial thermal conduction model inside the fuel pin to calculate material temperatures, and a thermal convection model in the cooling channel to calculate the coolant axial temperature distribution. The coolant temperature is calculated for each fuel assembly at each axial level using the convective model. These temperatures, in turn, are used to calculate the material temperatures in the fuel rods using the conduction model. Coolant and material temperatures are calculated for each assembly at each axial level. The average material temperatures are used to evaluate densities

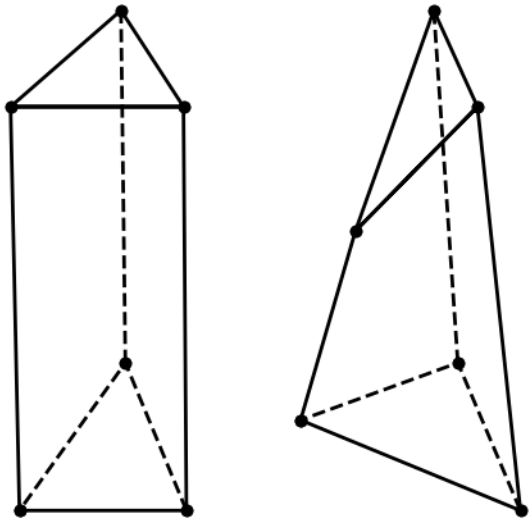

Figure 2.1 Wedge elements used in LMFR simulation [DP21]

and temperature-dependent cross sections [DP20]. As the temperatures change, a built-in thermal expansion model calculates the new finite element volumes and materials number densities to preserve the mass of material.

A depletion model has been recently added to LUPINE to enable fuel cycle studies [Pal21]. The model performs depletion for each individual assembly at different axial levels. LUPINE builds the depletion matrix and uses the Chebyshev Rational Approximation Method (CRAM) solver to solve it. Through the coupling of the depletion model with the neutronics, thermal hydraulic and thermal expansion models of LUPINE, the feedback from these physics is considered in the depletion calculation. With these capabilities, LUPINE can accurately calculate nuclide densities in the core through the fuel cycle.

The reactor description is provided for LUPINE through a user-friendly input file, through which the user can control the different conditions of the reactor. The input is keyword-based and organized into blocks. These blocks are either core-type or state-type. In the former, the geometry, material description and cross sections for the reactor are provided. The state-block is where commands and flags that control the type of solver, solver parameters, the calculation mode and the code output are provided. Additionally, LUPINE's input supports multiple statepoint calculations. This allows for easy handling of reactivity coefficients and depletion statepoint calculations.

LUPINE solves the applicable equations in a general geometry in either triangular or wedge elements. Such elements are shown in Fig. 2.1. LUPINE accepts the mesh in Visualization Toolkit (VTK) format. In this thesis, the preprocessing code HEXCORE code was utilized to generate the VTK files for the hexagonal reactor geometries. HEXCORE accepts inputs in DIF3D format. The code converts the description from ANIP format (i.e. similar to those used in DIF3D input) to VTK format.

Regions of the mesh are filled with smeared materials. This is a conventional practice in modeling and simulation of LMFRs since the neutron mean-free-path in fast reactors is significantly larger than materials dimensions. The mesh regions in the VTK file are given material numbers that are used to assign materials to the regions through the `LUPINE` input file. A visualization of a core mesh generated by `HEXCORE` is presented in Fig. 2.2. The different colors in the mesh represent different smeared materials filling the mesh elements.

The smeared material number densities are calculated using the fast reactor assembly pre-processing code `HEXBLD`. The code takes the fuel assembly geometry and material description through an input file and produces input files for MC^2-3. These inputs can be used to generate cross sections. Additionally, `HEXBLD` writes the smeared material number densities in include files which can be passed to the `LUPINE` input.

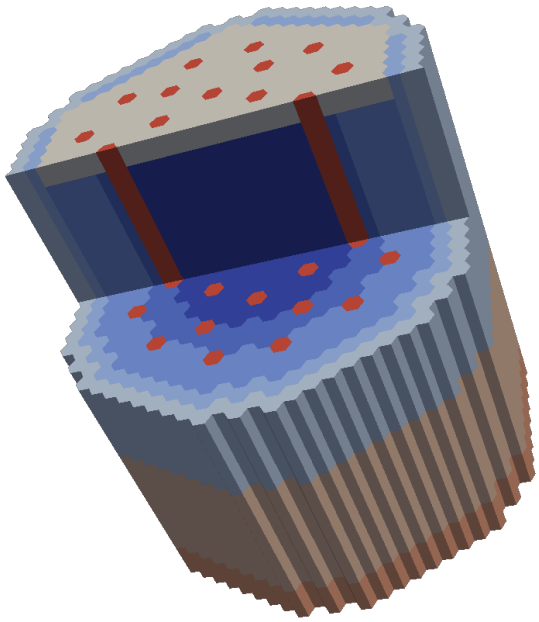

Figure 2.2 Full-core model generated by `HEXCORE`

Material cross sections can be provided using an ISOTXS file format or using input cards. In this thesis, MC^2-3 was utilized to generate ISOTXS files. MC^2-3 input files are prepared by the bundle pre-processing tool `HEXBLD`. A summary of the process of modeling and simulation of LMFRs using `LUPINE` is provided in Fig. 2.3

`LUPINE` supports the modeling of SFR materials through built-in material properties for sodium coolant, HT9 steel, and uranium with 10% (by weight) zirconium (U10Zr). Built-in material properties and models for lead coolant, UN fuel, corrosion resistant DS4 steel and mass flow distribution model have also been added. These include thermal hydraulic properties for lead, gap conductivity, UN fuel conductivity (as a function of porosity) and UN thermal expansion. These models and

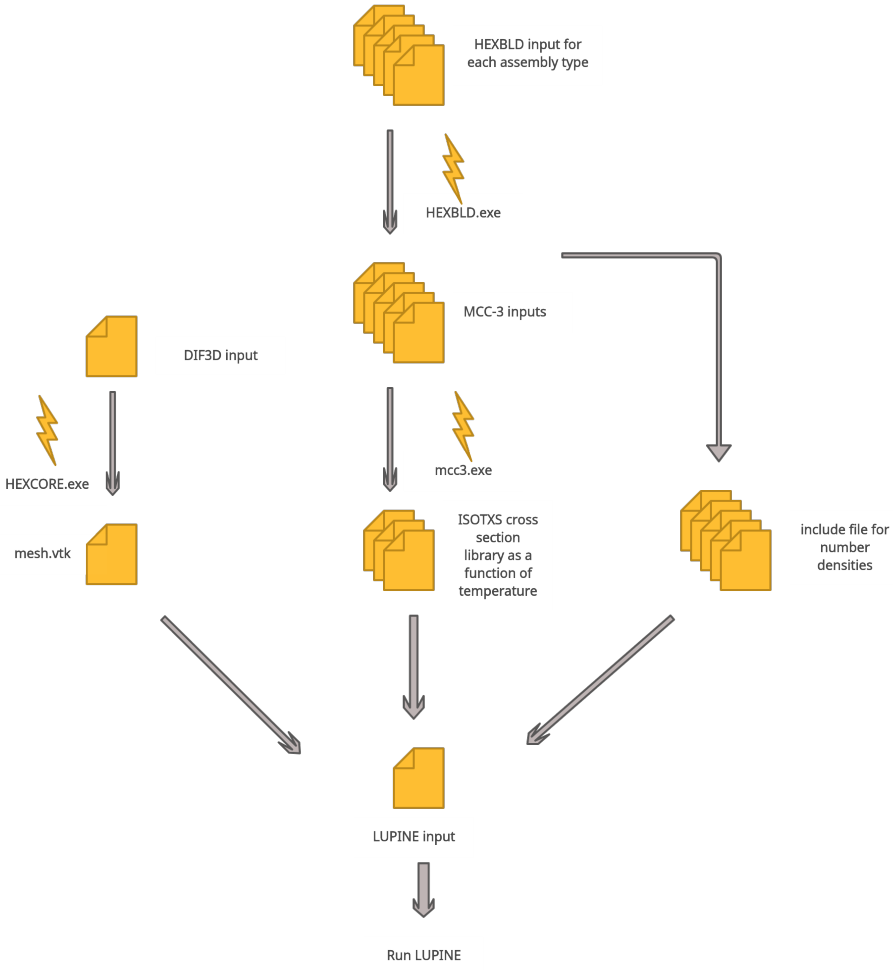

Figure 2.3 LMFR Simulation Tools

properties are described in detail in the upcoming sections.

2.2 Lead Coolant Thermal Properties

`LUPINE` utilizes a steady-state, one-dimensional, axial heat convection model to calculate bulk coolant temperatures axially within the channel. The code then utilizes a one-dimensional steady-state conduction model to calculate the fuel pin component temperatures at each axial level. Fig. 2.4 shows a visualization of the conduction and convection models that `LUPINE` solves. The convection model assumes no cross-flow between channels and ideal fluid mixing within a channel. Lead thermal properties required by the thermal hydraulic model in `LUPINE` are density (ρ), heat capacity (C_p), enthalpy (h), thermal conductivity (k), and dynamic viscosity (η). All of these properties are required as a function of coolant temperature and were obtained from [Sob12].

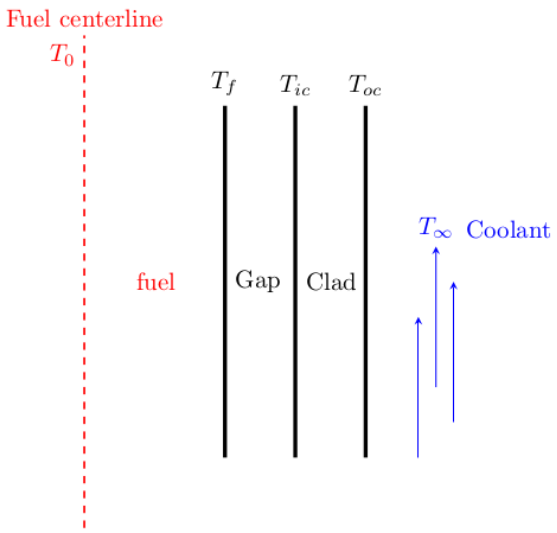

Figure 2.4 Thermal convection and thermal conduction models of `LUPINE`

The density of lead is given by Eq. 2.1 as:

$$\rho(T)\left[\frac{kg}{m^3}\right] = \rho_M - A_\rho \times (T - T_M) \tag{2.1}$$

where ρ_M is the density at normal melting temperature, A_ρ is a constant, T_M is the melting temperature of lead and T is the temperature at which the density is being calculated. At atmospheric pressure these two parameters have the values of 10671 $\left[\frac{kg}{m^3}\right]$ and 1.2795 $\left[\frac{kg}{m^3.K}\right]$, respectively. This correlation is valid for lead coolant in the range from melting temperature (600 [K]) to boiling temperature.

Lead temperature dependent heat capacity (C_p) is calculated using the following correlation:

$$C_p(T)\left[\frac{J}{K.mol}\right] = a + b\,T + c\,T^2 + d\,T^{-2}. \tag{2.2}$$

Table 2.1 presents the values of the coefficients in this correlation. The precision in the measurements of heat capacity for lead is satisfactory up to 1500 [K] (with a precision of about 5%).

Table 2.1 Lead Coolant Heat Capacity Correlation Coefficients [Sob12].

Parameter	Value
a $\left[\frac{J}{K.mol}\right]$	36.50
b $\left[\frac{J}{K^2.mol}\right]$	-1.02×10^{-2}
c $\left[\frac{J}{K^3.mol}\right]$	3.2×10^{-6}
d $\left[\frac{J.K^2}{mol}\right]$	-3.158×10^{5}

The change in lead enthalpy can be calculated by integrating the lead heat capacity formula as:

$$h(T)-h(T_M)=\int_{T_M}^{T} C_p(T)dT. \tag{2.3}$$

The thermal conductivity of liquid metals is a difficult quantity to measure. This is because of the heat convection in the liquid metal. Thermal conduction measurement for lead in the literature seem to agree well for temperatures close to the melting point. However, as the temperature increases, measurements seem to disagree. This was explained to be due to the presence of impurities, oxidation of liquid lead and experimental conditions [Han]. The thermal conductivity of lead at atmospheric pressure can be calculated using the correlation provided in Equation (2.4):

$$k(T)\left[\frac{W}{m.K}\right]=k(T_M)+A_k(T-T_M). \tag{2.4}$$

The coefficients in the correlation are given in Table 2.2.

Table 2.2 Lead Coolant Thermal Conductivity Correlation Coefficients [Sob12].

Parameter	Value
$T_M\,[K]$	600.8
$k_{Pb}(T_M)\left[\frac{W}{m.K}\right]$	15.8
$A_k\left[\frac{W}{m.K^2}\right]$	0.011

The dynamic viscosity of liquid lead can be calculated using the following Arrhenius-type equation:

$$\eta(T)[\text{Pa.s}]=\eta_\infty \exp\left(\frac{E_n}{RT}\right) \tag{2.5}$$

Where E_n is the activation energy of motion for viscous flow, R is the universal gas constant (8.314 $\left[\frac{J}{mol.K}\right]$), and T is the temperature in [K]. η_∞ is the asymptotic value of viscosity (η) as temperature grows very large (i.e. $T\rightarrow\infty$). The values for parameters in this equation for liquid lead are presented in Table 2.3.

Table 2.3 Lead Coolant Viscosity Correlation Coefficients [Sob12].

Parameter	Value
$\eta_\infty\,[Pa.s]$	0.455×10^{-3}
$E_n\,[J]$	8888

This correlation for the dynamic viscosity shows good agreement with the experimental data at

temperatures from the melting point up to 1270 [K].

All of the lead properties have been added to LUPINE and are used if the lead is selected as the reactor coolant in the LUPINE input file.

2.3 Uranium Mononitride Properties

Uranium mononitride (UN) is a candidate fuel for fast reactors, generally, and LFRs, specifically. It features advantages over other types of fuels. In comparison with oxide fuel, UN can achieve higher burnups and conversion ratios due to its higher fissile content [Ekb18]. It also has a higher thermal conductivity, better chemical stability with cladding material and coolants, better irradiation stability, and a better chemical compatibility with the PUREX reprocessing technique. In comparison with U10Zr metallic fuel, UN has a higher melting temperature, which leads to a larger safety margin. However, UN fuel also presents several challenges. For example, very limited in-pile experience exists with UN fuel. Also, the tendency of transuranic nitrides to dissociate at sintering temperature adds difficulty to the fabrication process. An additional challenge to UN is the high neutron absorption cross section of ^{14}N. The reaction (n,p) of ^{14}N results in the production of the radiotoxic ^{14}C. It also deteriorates the neutron economy of the core [Kim19]. These two problems can be solved by the enrichment of UN with ^{15}N. However, enrichment with ^{15}N results in 6% to 9% increase in the fabrication cost [Puk13]. Finally, UN poses some safety concerns due its decomposition that occurs above 2000 [^{o}C].

The thermal model of UN fuel in LUPINE includes the fuel thermal conductivity and fuel linear expansion factor as functions of temperature. Thermal conductivity of UN at 100% theoretical density can be described using the following correlation [Rog03]:

$$k_{UN,100}\left[\frac{W}{m.K}\right] = 1.37T^{0.41} \tag{2.6}$$

where T is in [K]. It should be noted that this correlation is based on the experimental data obtained by operating the research reactor BR-10 [Rog03]. The thermal conductivity of UN depends on porosity, so this effect has to be taken into account. This is performed by multiplying the thermal conductivity by the factor:

$$\frac{1-P}{1+P} \tag{2.7}$$

where, P is the volumetric fraction of pores in the fuel material.

Measurements of the thermal expansion of UN fuel have a large degree of uncertainty. Fortunately, the thermal expansion can be expressed using the lattice parameter of a material, and since the measurements of the lattice parameter of UN fuel have a smaller degree of uncertainty, they were used to develop the thermal expansion correlation as a function of temperature [Hay90].

$$\alpha\left[\frac{1}{K}\right] = 7.096\times10^{-6} + 1.409\times10^{-9}T. \tag{2.8}$$

LUPINE uses the linear expansion factor to model thermal expansion of the fuel. This is easily obtained by integrating Eq. 2.8 as

$$\begin{aligned} \alpha' &= \int_{298}^{T} \alpha(T) d\,T \\ &= 7.096 \times 10^{-6}(T-298) + \frac{1.409 \times 10^{-9}}{2}(T^2 - 298^2) \end{aligned} \tag{2.9}$$

UN properties have been added to LUPINE and are automatically used if the UN fuel is selected in the LUPINE input file.

2.4 Low-Swelling Austenitic Steel DS4

The selection of structural materials in LFRs is based on compatibility with coolant at different reactor conditions. Considering the tough environment of a fast reactor, structural materials should feature dimensional stability under irradiation. It is also required to possess favorable mechanical properties that must be retained under normal, abnormal and accident conditions. Corrosion issues can be avoided by reducing core outlet temperatures (i.e. maintain temperatures $< 773K$) [Kim18]. An alternative option is to utilize newly developed materials, which show promising corrosion resistance results. A candidate cladding material for LFRs is the double stabilized austenitic steel (DS4) [SL17] which is known for the low swelling behavior. However, the corrosion resistance of DS4 needs further demonstration for temperatures > 773 [K]. The composition of DS4 is presented in Table 2.4.

Table 2.4 Composition of DS4 [SL17].

Element	Cr	Ni	Mo	Mn	Si	C	Ti	Nb	V	Al	P	N	B
Composition (wt%)	14.7	25.5	1.28	1.48	0.82	0.057	0.12	0.13	0.03	0.013	0.029	0.018	0.0037

Unfortunately, there is no available literature describing DS4 physical and thermal properties. Thus, LUPINE utilized the composition of DS4 to model cladding and structural materials and imports the physical and thermal properties from HT9 library to build the thermal model for DS4.

2.5 Gap Conductivity Model

LMFRs with metallic fuel implement a bond region filled with liquid sodium in the region separating the fuel and cladding inner surface. Since liquid sodium has a higher thermal conductivity than a gas gap, this practice helps in keeping the fuel temperature below melting point in different reactor conditions. However, with other types of fuels, such as MOX and UN, the gap region is filled with an inert gas, such as helium. A visualization of the inner structures of a hexagonal-pitched fuel pin

with gap region is shown in Fig. 2.5

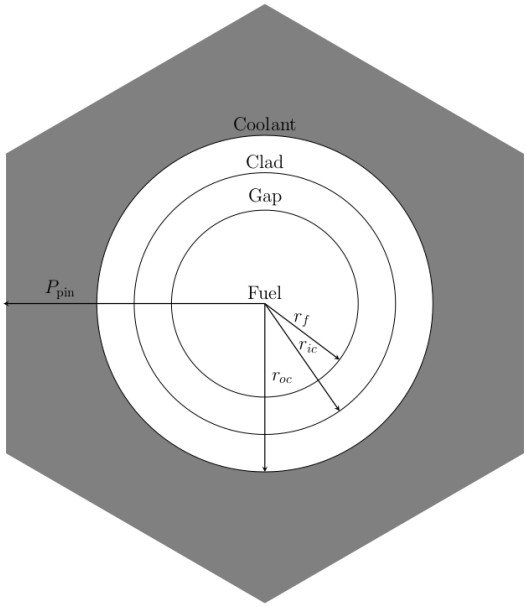

Figure 2.5 A visualization of a hexagonal-pitched fuel pin with gap region

The modeling of a gas gap region has been added to `LUPINE`. A simple steady-state, one-dimensional, radial gas gap thermal conduction model has been introduced. The common gap conductance concept used to model gap region conduction in LWRs was used to calculate the temperature drop across the gap region in `LUPINE`. Due to the lack of data regarding the gap conductance in LFR, a gap conductance of a PWR pin gap is used.

$$H\left[\frac{W}{m^2.K}\right] = 5680 \tag{2.10}$$

Then the effective gap conductivity can be calculated as:

$$h_g = H \times (r_{ic} - r_f) \tag{2.11}$$

The temperature drop across the gap can be calculated by considering the one-dimensional radial heat conduction equation.

$$\frac{1}{r}\frac{d}{dr}\left(h_g r \frac{dT}{dr}\right) = 0 \tag{2.12}$$

where the volumetric heat generation in the gap is equal to 0. Eq. 2.12 is solved by first multiplying by r and integrating over the radial domain $[r_f, r']$ with $r' \in [r_f, r_{ic}]$:

$$\int_{r_f}^{r'} \frac{d}{dr}\left(h_g r \frac{dT}{dr}\right) = 0 \tag{2.13}$$

$$h_g r' \left.\frac{dT}{dr}\right|_{r'} - h_g r_f \left.\frac{dT}{dr}\right|_{r_f} = 0 \tag{2.14}$$

The heat flux at the fuel pellet surface can be written in terms of the fuel volumetric heat generation as follows.

$$r_f h_g \left.\frac{dT}{dr}\right|_{r_f} = -\frac{q''' r_f^2}{2} \tag{2.15}$$

Note that

$$h_g \left.\frac{dT}{dr}\right|_{r_f} = -q'' \tag{2.16}$$

and

$$2\pi R q'' = \pi R^2 q''' \tag{2.17}$$

Substituting Eq. 2.15 in Eq. 2.14 results in.

$$h_g r' \left.\frac{dT}{dr}\right|_{r'} + \frac{q''' r_f^2}{2} = 0 \tag{2.18}$$

By dividing the equation by r'.

$$h_g \left.\frac{dT}{dr}\right|_{r'} + \frac{1}{r'}\frac{q''' r_f^2}{2} = 0 \tag{2.19}$$

$$h_g \frac{dT}{dr'} + \frac{1}{r'}\frac{q''' r_f^2}{2} = 0 \tag{2.20}$$

Multiple by dr'

$$h_g dT(r') + \frac{1}{r'}\frac{q''' r_f^2}{2} dr' = 0 \tag{2.21}$$

Integrating Eq. 2.22 over the domain $[r_f, r]$ where $r \in [r_f, r_{ic}]$.

$$\int_{r_f}^{r} h_g dT(r') + \int_{r_f}^{r} \frac{1}{r'}\frac{q''' r_f^2}{2} dr' = 0 \tag{2.22}$$

$$h_g \left(T(r) - T(r_f)\right) + \frac{q''' r_f^2}{2} \ln\left(\frac{r}{r_f}\right) = 0 \tag{2.23}$$

Solving the equation for $T(r)$:

$$T(r) = T(r_f) - \frac{q''' r_f^2}{2h_g} \ln\left(\frac{r}{r_f}\right) \tag{2.24}$$

It should be noted that this derivation assumes constant gap conductance. One suggestion for future work is to add a gap conductance model that is a function of burnup and considers the physics of the fuel swelling and clad creep.

2.6 Mass Flow Distribution

In LMFRs, the coolant mass flow in fuel assemblies is controlled using orifices. This is designed to limit coolant flow from going to low powered assemblies with low flow resistance. In order to make such a control available in simulating LMFRs, the LUPINE mass flow distribution model has been modified to account for user supplied assembly mass flow multipliers.

The user provides a set of mass flow multipliers f_i and the assembly index that is used to link the multiplier to the correct assembly location in the mesh. The multipliers are normalized such that the sum of the multipliers is equal to the number of assemblies as in Eq. 2.25

$$F_i = N \frac{f_i}{\sum_i f_i} \tag{2.25}$$

where i is the assembly index and N is the number of assemblies. F is the i^{th} assembly normalization factor that preserves the total flow in the core. After that, the normalized multipliers are applied to the flow area of the channel $A_{cool,i}$ as

$$A_{cool,i} = A_{cool,i} \times F_i \tag{2.26}$$

Then the mass flow distribution in assembly i is calculated as

$$\dot{m}_i = \dot{m}_{Rx} \frac{A_{cool,i}}{A_{cool,Rx}} \tag{2.27}$$

It should be noted that the mass flow distribution multipliers are all set to 1 by default.

2.7 Summary

In this chapter, the capabilities that enable the modeling and simulation of LFRs in LUPINE have been introduced. These included introducing the lead thermal properties, UN thermal expansion and thermal conductivity models, a gas gap region model and mass flow distribution model.

The lead thermal property correlations have been discussed. The ranges of applicability of the correlations has been presented. The UN thermal expansion and thermal conductivity correlations have been presented. Porosity effect on UN thermal conductivity has been discussed, too. As a gas gap region is typically used with non-metal fuels, gap model was derived. Finally, the mass flow distribution model that allows realistic modeling of fuel assembly coolant flow distribution has been introduced. All these models have been incorporated in LUPINE.

CHAPTER

3

OPTIMIZATION METHODOLOGY

3.1 Introduction

As discussed in Section 1.4, the core design and optimization process is an iterative process that considers neutronics, thermal hydraulics, structural mechanics and economics. In an attempt to make the process of designing and optimizing LMFRs easier, this project introduces the Design and Optimization Methodology (DOM). DOM is a general purpose methodology designed to enable the efficient exploration of a search space. It achieves this by utilizing the design of computer experiment approach to perform efficient sampling of the search space, and the physics based identification of samples from the search space that represent invalid designs.

The methodology is based on a design of computer experiment, or shortly Design Of Experiment (DOE), approach to perform a search on the design space of a reactor core (hereon referred to as search space). To clarify, a DOE can be defined as the process of systematic selection of a process input variable instances at which to run a computer simulation [San03]. It is usually used to help identify the inputs that have most influence on a process or phenomena.

The goal of DOM can as summarized by efficiently exploring a search space to identify regions of the search space where the potential optimum design is located. In this chapter, the methodology and its application will be presented.

As a proof of concept of DOM, an application of the methodology has been attempted. In order to automate the application of DOM, a Python program was written. The theory of the program and its modules will be presented in detail in this chapter. The program was constructed to perform an optimization for a long-life core LFR fueled by UN. However, extending the program to include other LMFR coolants and fuel materials is straightforward. It should be noted that the application of DOM

presented in this work leverages the multiphysics modeling and simulation capabilities of LUPINE to reliably investigate a search space and come up with an optimized core design. Additionally, the Python program was equipped with an economic analysis module that calculates the LCOE and incorporates it in the decision making process.

3.2 The Design and Optimization Methodology (DOM)

Computer models of physics phenomena are becoming increasingly available with increasing computing power. Such models are also cheaper to run and experiment with compared to physical experiments. This is especially true when the problem being investigated has a large input space. For these reasons, computer codes simulating physical phenomena have been widely used as a proxy for physical systems for problems where a large number of experiments needs to be conducted. Optimization problems are no exception since a large number of experiments or simulations are needed to identify an optimal configuration.

Depending on the nature of variables constituting the search space (hereon referred to as explanatory variables), the optimization problem can be classified into continuous or discrete. When the explanatory variables of a search space take discrete values, the result is a discrete optimization problem. An example of such an optimization is the LWR core loading pattern design problem. The explanatory variables for this problem are usually the number of fuel assembly types and the number of allowed fuel locations in the core. Assuming there are a finite number of fuel assembly types and fuel locations, the number of possible designs in the search space is finite, although it can be very large (as large as 10^{31} possibilities). On the contrary, when the explanatory variables are allowed to take on a continuous range of values, we formulate a continuous optimization problem. The number of possible designs is infinite which makes it impossible to explore all possible designs in the search space. An example of such a case is finding the optimum enrichment distribution and assembly geometry in a reactor core.

A traditional engineering procedure for exploring a search space is the factorial design which can be performed in full or fractional factorial styles. If the explanatory variables are continuous, each one is divided into n_i bins (also called levels) to allow limiting the search space size. In a full factorial design, one design is constructed for every possible combination of explanatory variables and levels. Fig. 3.1 shows a full factorial design for a bi-variate search space with five bins for each explanatory variable, which leads to 25 total samples. Each point of the grid in the figure represents a single sample in the design space. Such a sample will be referred to as design sample from here on.

The number of design samples in a full factorial design can be calculated as

$$\text{No. trials} = n_1 \times n_2 \times ... \times n_I \tag{3.1}$$

where I is the number of explanatory variables and n_i is the number of bins for variable i. The number of trials in a factorial design can grow very large, rendering the problem computationally prohibitive. For this reason, the DOE approach is usually suggested as a way to potentially alleviate

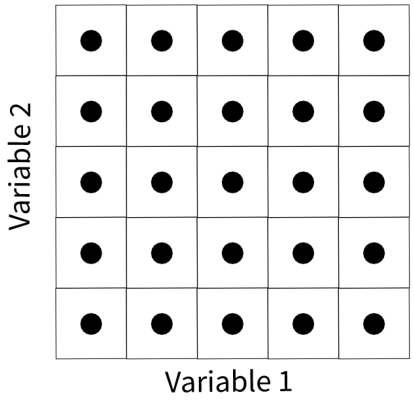

Figure 3.1 Every possible combination in a bi-variate search space

the computational cost associated with search space exploration. This is especially important when the model describing the input-output relationship takes long times to run.

Of special interest among the DOE methods are the space-filling (also known as exploratory) designs. These designs allow for evenly spreading the generated samples across the search space to attain optimal space coverage. Such designs can help in efficiently exploring a search space with a reduced computational effort which aligns with DOM goals.

The ultimate goal of DOM is to enable the efficient exploration of a search space. The methodology attempts to achieve this by two means. The first is performing efficient sampling of the search space. This is done by utilizing a Latin Hypercube Sampling (LHS) technique, which is one of the space-filling designs in DOE. The second is the on-the-fly identification of regions in the search space that hosts impractical designs and excluding designs in these regions from further processing using computationally expensive multiphysics codes.

In DOM, the design process starts by selecting the objectives, technology of interest, materials applicable to the particular technology, and technology constraints. The designer also sets up the domain of the search space by identifying the explanatory variables and the range of values they can take. After that, DOM attempts to sample the explanatory variable within the specified ranges. The methodology follows that by performing an on-the-fly screening for the generated design samples and preliminarily evaluates their compliance with reactor design constraints. After that, designs that are shown invalid by the screening process are eliminated from further processing. Designs successfully passing the screening are flagged, and a multiphysics analysis is carried out for them. In the last step of the process, based on the multiphysics results, the optimum design is identified from the flagged designs.

This methodology has been applied to a case study on a long-life core LFR design. The goal is to use DOM to optimize the original core design. A Python program was used to automate the application of the methodology. Although the program was prepared to apply DOM for a LFR fuel by UN, the extension of the program to include different LMFR coolants and fuel materials is straightforward. In the following discussion, the details of the effort to apply DOM will be presented.

3.3 Optimization of LFR using DOM

As mentioned earlier, a Python program was implemented to apply DOM to optimize a long-life core LFR. This section presents the details of this program. A summary of the process of using DOM is as follows.

In the beginning of the DOM, the domain of the search space, reactor power, assumed power peaking factors and design constraints are provided through an input file. In the particular case of the long-life LFR core investigated in this work, the objective of the design process is to achieve the lowest fuel cycle cost while maintaining compliance with core constraints.

The Python program receives the domain of the search space and generates N samples using LHS. In the screening process, the identification of the invalid design samples is achieved by utilizing a simple thermal hydraulic model of the hottest fuel channel in the reactor. The model is composed of one-dimensional steady-state axial convection and radial conduction models. The solution of these two models results in calculated coolant and fuel pin component temperatures. The temperatures are compared against the design constraints to determine if the design is sound from a thermal-hydraulic point of view. Finally, a flag is returned to describe the status of the design sample (i.e. valid or invalid).

Upon finishing the screening, designs for which component temperatures exceed design limits are discarded. For cases that show compliance with the constraints, a full reactor model is prepared for multiphysics analysis using `LUPINE`. This is done in four steps. First, the geometry of the fuel assembly is calculated. Second, the Python program builds inputs for `HEXBLD` and executes the code. This is followed by a third step of building the mesh using `HEXCORE` and supplying it to `LUPINE` input. In the last step, the `LUPINE` input is built for the particular case.

Once the mesh is constructed, `LUPINE` input is built and the code is executed. Once all the successful cases are run with `LUPINE`, the Python program will analyze the results of each case and applies another screening to them. The process compares the designs to the design constraints again. If the design violates the constraints, it will be excluded from further processing. Otherwise, the cost function for the design sample will be calculated. The reactor with the smallest cost function among the successful design samples will be selected to be the optimal core. A summary of the steps to apply DOM to optimize the long-life core LFR is presented in Fig. 3.2.

In the subsections to follow, the details of the Python program written for optimizing the long-life core LFR will be presented.

3.3.1 Latin Hypercube Sampling

LHS is a space-filling DOE technique aiming to generate evenly-spread design samples across a search space. The theory behind the LHS is presented in this subsection.

Assume that we are interested in sampling p points from a d-dimensional space. The matrix $\mathbf{X} = \left[\mathbf{x_1}, \mathbf{x_2}, ...\mathbf{x_p}\right]^{\mathbf{T}}$ represents the total samples. Row $\mathbf{x}_i = \left[x_i^{(1)}, x_i^{(2)}...x_i^{(d)}\right]$ represents the i^{th} sample. The LHS algorithm divides each dimension of the d-dimensional space into p strata with marginal

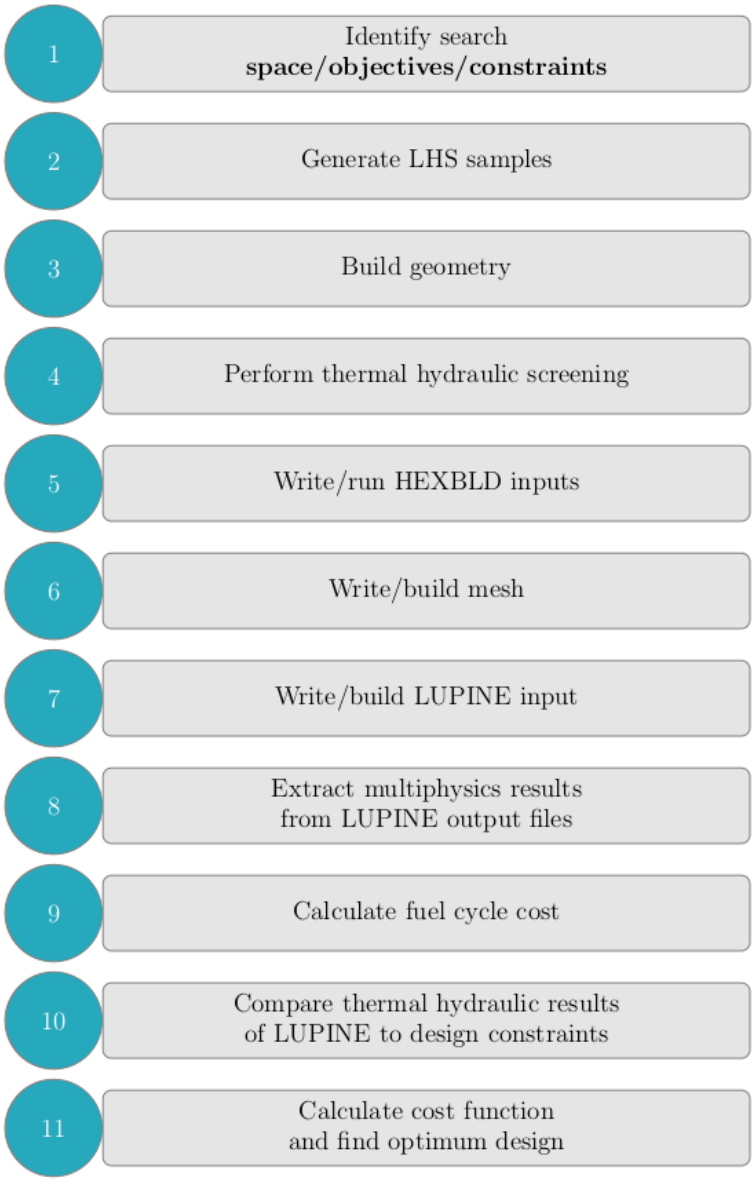

Figure 3.2 Summary of design and optimization methodology

probability of $1/p$ on a square grid and samples the design parameters such that there is only one sample in each bin (i.e. called Latin Hypercube) [Mck79]. To simplify the discussion, this concept is demonstrated for a bi-variate design space as in Fig. 3.3. Assuming that we want to withdraw five samples from this space. We notice that the search space is made up of a 5×5 grid and there is only one design sample per row and one design sample per column. This is called a latin square since it is in 2-dimensional space. The generalization of this concept to a d-dimensional space is the LHS.

Compared to regular sampling, LHS can be used to sample the space more effectively for a certain budget of samples. Fig. 3.4 shows a comparison between LHS and regular sampling method

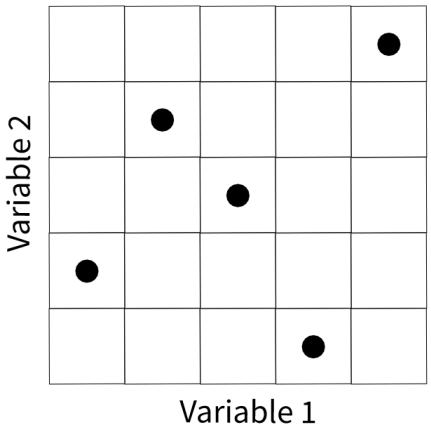

Figure 3.3 Latin square sample

in sampling a bi-variate design space from which 50 samples are withdrawn.

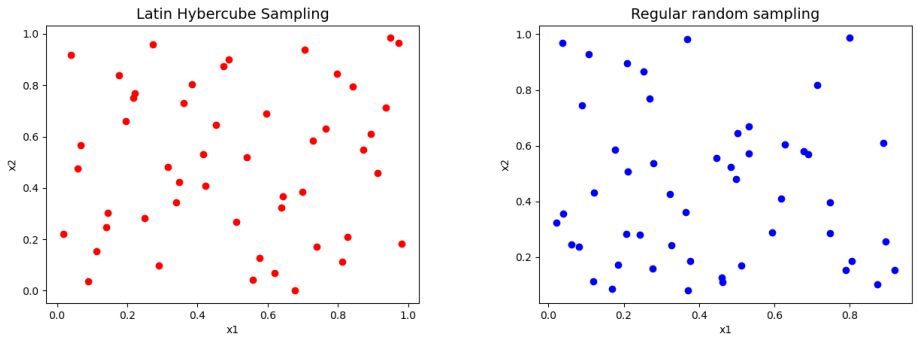

(a) **(b)**

Figure 3.4 Comparison between (a) LHS and (b) Regular sampling

3.3.2 Long-Life Core LFR Search Space

To construct a search space, the explanatory variables constituting the search space must be identified. As an example, in this project, the WEC long-life core LFR [Kim19] was adopted to demonstrate DOM. For this particular case the search space was constructed based on six explanatory variables. Four of these are geometric explanatory variables; the pin radius R, Pitch to Diameter ratio (P/D), fuel height L and assembly pitch P_{Assembly}. It should be noted that the WEC long-life core LFR core has three regions in the core. These are the inner core, middle core and outer core regions. The regions are defined based on the fuel enrichment. The inner core and middle core enrichment were also chosen to be explanatory variables. The outer core enrichment was calculated such that it stays

higher than the inner and middle core enrichments, but does not exceed the limit defining the low enriched fuel (i.e. 19.9%).

It should be noted that the selection of the explanatory variables was based on both a literature review and performing computer experiments which helped in understanding the sensitivity of the design to these variables.

The Python LHS sampling package was utilized to generate the multivariate samples [DD12] [Moz20]. The package generates the samples ζ_i in the interval $[0,1]$. Assuming that an explanatory variable X is to be sampled in the range $[X_{min}, X_{max}]$, the sample X_i will be

$$X_i = X_{min} + \zeta_i (X_{max} - X_{min}) \tag{3.2}$$

3.3.3 Geometry Calculator

For each sample produced by the LHS function, the geometry calculator is used to reveal details of the geometry of the fuel assembly based on the design sample. The goal of this calculator is to calculate how many fuel pins fit inside the fuel assembly given the assembly size and fuel pin pitch. This is done through an iterative process that compares the length of the diagonal of the inner duct in a fuel assembly with the sum of fuel pin pitches across the diagonal.

Knowing that a hexagon is composed of six equilateral triangles, the diagonal of the inner duct $d_{\text{corner-to-corner}}$

$$d_{\text{corner-to-corner}} = 2a \tag{3.3}$$

where a is the side length of the hexagon inside at the inner side of the duct as shown in Fig. 3.5. The side length a can be calculated based on the Pythagorean rule as

$$\left(\frac{a}{2}\right)^2 + \left(\frac{P_{\text{inner duct}}}{2}\right)^2 = a^2 \tag{3.4}$$

rearranging the equation gives

$$a = \sqrt{\frac{P_{\text{inner duct}}^2}{3}} \tag{3.5}$$

which results in

$$d_{\text{corner-to-corner}} = 2a = 2\sqrt{\frac{P_{\text{inner duct}}^2}{3}} \tag{3.6}$$

The inner duct flat-to-flat pitch is calculated as

$$P_{\text{inner duct}} = P_{\text{Assembly}} - G_{\text{Assembly}} - 2 \times t_{\text{duct}} \tag{3.7}$$

where $P_{\text{inner duct}}$ is the inner duct flat-to-flat pitch, P_{Assembly} is the assembly pitch, G_{Assembly} is the inter-assembly gap thickness, and t_{duct} is the assembly duct thickness. In the Python program, the

assembly duct thickness is calculated based on a fixed duct thickness ratio DTR defined as

$$\mathrm{DTR} = \frac{t_{\mathrm{duct}}}{P_{\mathrm{Assembly}}} \tag{3.8}$$

Fig. 3.5 shows a demonstration of the dimensions discussed earlier.

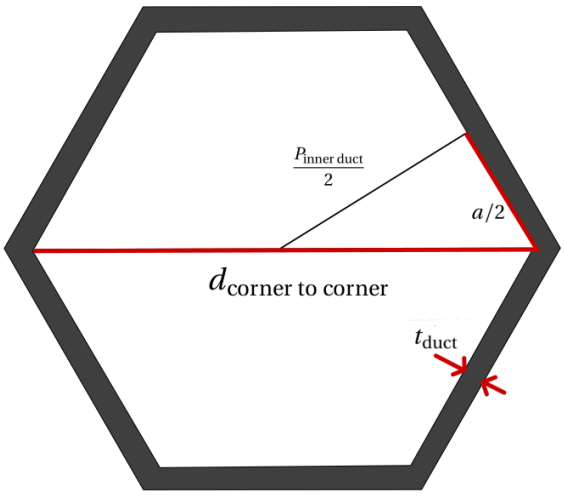

Figure 3.5 Top view hexagonal assembly

Once these dimensions have been calculated for the design sample, the iterative process of calculating the number of fuel pins per assembly starts. Initially, the assembly is assumed to contain one fuel pin. The pin pitch P_{pin} is compared to the diagonal length $d_{\text{corner-to-corner}}$. If the diagonal length is larger, another ring of fuel pins is added to the assembly. After that the sum of fuel pin pitches across the diagonal is calculated as

$$d_{\mathrm{pitches}} = \sum_{i=1}^{N} P_{\mathrm{pin}} \tag{3.9}$$

where N is the count of fuel pins across the diagonal of the hexagon. d_{pitches} is compared to $d_{\text{corner\_to\_corner}}$ again. The process of adding rings continues until d_{pitches} exceeds $d_{\text{corner-to-corner}}$. At this point, the number of rings will be reduced by one and the number of fuel pins in a fuel assembly is calculated as

$$N_{\mathrm{pins}} = 3n(n-1)+1 \tag{3.10}$$

Fig. 3.6 demonstrates the process visually. Algorithm 1 presents a pseudo code for performing this iterative process.

The last task that the geometry function performs is the calculation of the coolant flow cross sectional area, the wetted perimeter and the hydraulic diameter of the assembly. The assembly flow

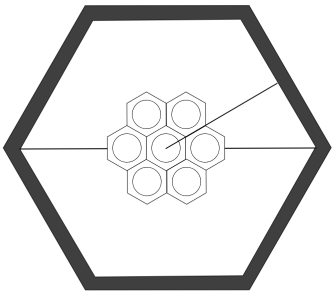

Figure 3.6 The iterative process to calculated number of pins in the fuel assembly

cross sectional area was calculated as the total area of inside the inner duct ($A_{x,1}$) minus the cross sectional area of the fuel pins ($A_{x,2}$)

$$\begin{aligned} A_{x,1} &= 12 \times \frac{1}{2} \times \frac{a}{2} \times \frac{P_{\text{inner duct}}}{2} \\ &= \frac{3}{2} a P_{\text{inner duct}} \end{aligned} \tag{3.11}$$

$$A_{x,2} = N_{\text{pins}} \times \pi R_{\text{pin}}^2 \tag{3.12}$$

where R_{pin} is the fuel pin radius.

The total assembly wetted perimeter can be calculated as the sum of wetted perimeter of the fuel pins ($P_{w,1}$) plus the periphery of the inner duct.

$$P_{w,1} = 2\pi R_{pin} N_{\text{pins}} \tag{3.13}$$

$$P_{w,2} = 6a \tag{3.14}$$

Finally, the hydraulic diameter is calculated as follows

$$D_e = \frac{4A_x}{P_w} \tag{3.15}$$

3.3.4 Thermal Hydraulic Screening Using the Hottest Channel Model

The goal of the thermal hydraulic screening is to quickly identify design samples in the search space that do not meet the thermal hydraulic constraints and exclude them from computationally expensive multiphysics analysis. Based on assumptions of the radial (r_p) and axial (r_z) power peaking factors (which the user provides through an input file), the hottest fuel channel is directly modeled

Algorithm 1: Calculating the number of fuel pins in an assembly

Result: Number of rings in fuel assembly
initialization;
nrings_converged = **False**;
nrings = 0;
$d_{\text{corner-to-corner}}$;
while *(**not** nrings_converged)* **do**
    nrings = nrings + 1;
    $n_{\text{pins across diagonal}} = 2 \times \text{nrings} - 1$;
    $d_{\text{pitches}} = n_{\text{pins across diagonal}} \times P_{pin}$;
    if $(d_{pitches} >= d_{corner\text{-}to\text{-}corner})$ **then**
        nrings_converged = **True**;
        nrings = nrings − 1;
    end
end

using a one-dimensional steady-state axial convection and radial conduction models. The user can control the value of the power peaking factors to control the number of patterns excluded. This can be used to validate assumptions. Based on these, the component temperatures of the hottest channel are calculated and compared to the constraints set for the LFR technology of interest. If the constraints are met by the design sample, a full reactor model is built and analyzed by the multiphysics code `LUPINE`. Otherwise, the design sample is discarded. It should be noted that the user provided peaking factors are only used for the screening process (i.e. not in the `LUPINE` multiphysics solution).

The maximum and average linear power densities are related to the radial and axial peaking factors as

$$r = r_p \times r_z = \frac{q'_o}{q'_{\text{avg}}} \tag{3.16}$$

where q'_o and q'_{avg} are the maximum and reactor average linear power densities in the core, respectively. To model the hottest channel, a chopped cosine function is assumed to model the axial linear power density. This axial linear power shape is defined then as

$$q'(z) = q'_o \cos\left(\frac{\pi z}{L\chi}\right) \tag{3.17}$$

where χ is the converted axial peaking factor. χ is calculated based on the definition of the axial peaking factor.

To calculate χ let's first consider the average linear power density for the hottest channel $q'_{\text{avg,o}}$ is calculated as

$$q'_{\text{avg,o}} = \frac{1}{L}\int_{-\frac{L}{2}}^{\frac{L}{2}} q'(z)dz = \frac{1}{L}\int_{-\frac{L}{2}}^{\frac{L}{2}} q'_o \cos\left(\frac{\pi z}{\chi L}\right) \tag{3.18}$$

$$q'_{\text{avg,o}} = \frac{1}{L}\frac{\chi L q'_o}{\pi}\sin\left(\frac{\pi z}{\chi L}\right)\Bigg|_{-\frac{L}{2}}^{\frac{L}{2}} \tag{3.19}$$

$$q'_{\text{avg,o}} = \frac{2q'_0\chi}{\pi}\sin\left(\frac{\pi}{2\chi}\right) \tag{3.20}$$

Using this, the average linear power density q'_{avg} in the core can be calculated as

$$q'_{\text{avg,o}} = q'_{\text{avg}} r_p \tag{3.21}$$

By substituting Eq. 3.20 in Eq. 3.21

$$\frac{2q'_0\chi}{\pi}\sin\left(\frac{\pi}{2\chi}\right) = r_p q'_{\text{avg}} \tag{3.22}$$

Substituting r_p from Eq. 3.16 into this equation, we get

$$r_z = \frac{\pi}{2\chi\sin(\frac{\pi}{2\chi})} \tag{3.23}$$

Finally, χ is obtained by solving Eq. 3.23 and the axial distribution of the linear power density is constructed.

The average core linear power density can be calculates as

$$q'_{\text{avg}} = \frac{P_{\text{Rx}}}{L_c} \tag{3.24}$$

where P_{Rx} is the reactor thermal power, and L_c is the total fuel pins height in the core calculated as

$$L_c = N_{\text{pins}} L \tag{3.25}$$

where N_{pins} is the number of fuel pins in the reactor. For a hexagonal fuel assembly, Eq. 3.25 becomes

$$L_c = n_a L[3n(n-1)+1] \tag{3.26}$$

where n_a is the number of fuel assemblies in the core, and n is the number of fuel rings in the fuel assembly. Using this in Eq. 3.16 results in

$$q'_o = r_p r_z q'_{\text{avg}} = r_p r_z \frac{P_{\text{Rx}}}{L_c} \tag{3.27}$$

By this, the chopped cosine function is defined and the modeling of the hottest channel can be performed.

For the hottest channel, the fuel pin is divided axially into K axial zones as shown in Fig. 3.7. Knowing the linear power density function, an energy balance is applied on zone $j \in [1, K]$ to calculate the zone coolant outlet temperature. It should be noted that the core coolant inlet temperature

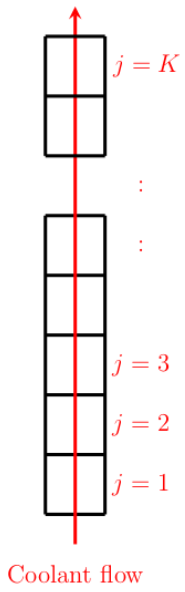

Figure 3.7 Axial discretization of a fuel pin

is known and the outlet of zone j is the inlet of zone $j+1$. Therefore, by applying the energy balance starting at node $j = 1$ and progressively marching upward in the channel, the rest of the node inlet and outlet temperatures can be calculated.

To calculate the axial zone outlet temperature, a simple energy balance on the domain $T' \in [T_{j,in}, T_{j,z'}]$ where $z' \in [z_{j,in}, z_{j,out}]$ is applied as follows.

$$\dot{m} \int_{T_{j,in}}^{T_j(z)} C_p(T) d\,T = \int_{z_{j,in}}^{z'} q'_o \cos\left(\frac{\pi z}{\chi L}\right) dz \tag{3.28}$$

A single axial zone flow model is shown in Fig. 3.8. By selecting the axial zone height to be small

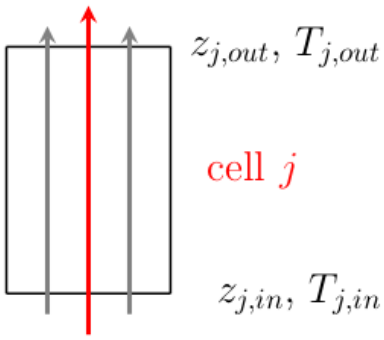

Figure 3.8 Single axial cell model

enough, the heat capacity $C_p(T)$ can be assumed to be constant along the zone. This results in

$$\dot{m} C_p(T_{j,in}) \int_{T_{j,in}}^{T_j(z')} dT = \int_{z_{j,in}}^{z'} q'_o \cos\left(\frac{\pi z}{\chi L}\right) dz \tag{3.29}$$

$$\dot{m} C_p(T_{j,in})\left[T_j(z') - T_{j,in}\right] = \frac{q'_o \chi L}{\pi}\left(\sin\left(\frac{\pi z'}{\chi L}\right) - \sin\left(\frac{\pi z_{j,in}}{\chi L}\right)\right) \tag{3.30}$$

By rearranging the equation, the axial zone $T_{j,out}$ outlet temperature can be calculated based on the following equation:

$$T_j(z') = T_{j,in} + \frac{q'_o \chi L}{\pi \dot{m} C_p(T_{j,in})}\left(\sin\left(\frac{\pi z'}{\chi L}\right) - \sin\left(\frac{\pi z_{j,in}}{\chi L}\right)\right) \tag{3.31}$$

The average coolant temperature in zone j is calculated as:

$$T_{j,avg} = \frac{1}{L_j} \int_{z_{j,in}}^{z_{j,out}} T_j(z) dz \tag{3.32}$$

The flow area of the fuel channel can be calculated as

$$A_{x,\text{channel}} = \frac{\sqrt{3}}{2} P_{\text{pin}}^2 - \pi R_{\text{pin}}^2 \tag{3.33}$$

Then, the mass flow rate in Eq. 3.31 can be calculated for the single fuel pin as

$$\dot{m} = \rho(T_{j,in}) \times A_{x,\text{channel}} \times v \tag{3.34}$$

where $\rho(T_{j,in})$ is the density of the coolant at inlet temperature and v is the coolant velocity in the channel.

In each node, the convection model is used to calculate the outer cladding temperature T_{oc}. The heat convection model at the clad outer surface can be expressed as follows:

$$q''_{oc} = h(T_{oc} - T_\infty) \tag{3.35}$$

Where q''_{oc} is the heat flux at the cladding surface (i.e. r_{oc}), T_∞ is the coolant bulk temperature (i.e. $T_\infty = T_{j,\text{out}}$) and h is the heat transfer coefficient. The relationship between the heat flux and linear power density at the cladding outer surface can be expressed according to

$$q''_{oc} = \frac{q'}{2\pi r_{oc}} \tag{3.36}$$

Substituting this into Eq. 3.35 and rearranging, the cladding surface temperature can be expressed as

$$T_{oc} = T_{j,\text{out}} + \frac{q'_j}{2\pi h} \tag{3.37}$$

The heat transfer coefficient h can be calculated as

$$h = \frac{\mathrm{Nu} \times k(T_{j,\mathrm{out}})}{D_e} \tag{3.38}$$

Where Nu is the Nusselt number (a dimensionless quantity). The Nusselt number can be obtained from the Subbotin-Ushakov correlation [PS07]. This correlation can be used to calculate the heat transfer coefficient of lead coolant in triangular fuel bundle.

$$\mathrm{Nu}_j = 7.55\frac{P}{D} - 20\left(\frac{P}{D}\right)^{-13} + \frac{3.67}{90\left(\frac{P}{D}\right)^2} \times \mathrm{Pe}^{0.56+\times 0.19\times \frac{P}{D}} \tag{3.39}$$

where $\frac{P}{D}$ is the pin pitch to diameter ratio. The correlation is valid for $1 < \mathrm{Pe} < 4000$ and $1.2 \leq \frac{P}{D} \leq 2.0$ according to [PS07]. [Mik09] presented Eq. 3.39 and confirmed that it is valid on $30 < \mathrm{Pe} < 5000$ and $1.1 \leq \frac{P}{D} \leq 1.95$. The author also confirmed that this correlation can be used to calculate the heat transfer coefficient of liquid metals (including lead coolant).

In Eq. 3.39, Pe is the Peclet number. It can be calculated as

$$\mathrm{Pe}_j = \mathrm{Re}_j \times \mathrm{Pr}_j \tag{3.40}$$

where Re is the Reynolds number which can be calculated as

$$\mathrm{Re}_j = \frac{\rho(T_{j,\mathrm{out}})\nu D_e}{\eta(T_{j,\mathrm{out}})} \tag{3.41}$$

and Pr is the Prandtl number and can be calculated as

$$\mathrm{Pr}_j = \frac{\eta(T_{j,\mathrm{out}})C_p(T_{j,\mathrm{out}})}{k(T_{j,\mathrm{out}})} \tag{3.42}$$

The zone inlet temperature is used to calculate the dimensionless quantities Reynolds number **Re**, Prandtl number **Pr**, Peclet number **Pe** and Nusselt number **Nu** at zone j. where ρ is the density, $T_{j,\mathrm{out}}$ is the zone coolant outlet temperature, ν is the coolant velocity, D_e is the channel hydraulic diameter, η is the lead viscosity. where C_p is the heat capacity and k is the conductivity.

By using the outer cladding temperature, a one-dimensional conduction model is used to progressively calculate the inner cladding surface temperature, the fuel surface temperature and the fuel centerline temperature. The fuel pin structure used in this procedure is shown in Fig. 2.5 The heat conduction equation inside the cladding can be describes as

$$\nabla \cdot (k_c \nabla T_B(r)) = 0 \tag{3.43}$$

For cylindrical geometry, it becomes

$$\frac{1}{r}\frac{d}{dr}\left(r k_c \frac{dT}{dr}\right) = 0 \tag{3.44}$$

The solution for this equation has been presented earlier in Section 2.5 for the gap region. The solution for the clad region is analogous. Therefore, the temperature drop across the clad will satisfy

$$T_{ci} - T_{co} = \frac{q'}{2\pi k_c} \ln\left(\frac{r_{oc}}{r_g}\right) \tag{3.45}$$

Additionally, based on the discussion presented in Section 2.5, the steady-state, one-dimensional, radial thermal conduction equation and the temperature drop across the gap region are presented in Eq. 3.46 and Eq. 3.47:

$$\nabla \cdot \left(h_g \nabla T_B(r)\right) = 0 \tag{3.46}$$

$$T_f - T_{ic} = \frac{q'}{2\pi h_g} \ln\left(\frac{r_{ic}}{r_f}\right) \tag{3.47}$$

The steady-state, one-dimensional, radial conduction equation in the fuel region is expressed as follows

$$\nabla \cdot \left(k_f \nabla(T_f)\right) + q''' = 0 \tag{3.48}$$

For one-dimensional cylindrical geometry, the conduction equation becomes

$$\frac{1}{r}\frac{d}{dr}\left(r k_f \frac{dT_f}{dr}\right) + q''' = 0 \tag{3.49}$$

multiplying by r and integrating over the over r in the range $[0, r_f]$

$$\int_0^{r'} \frac{d}{dr}\left(r k_f \frac{dT_f}{dr}\right) dr + \int_0^{r'} q''' dr = 0 \tag{3.50}$$

where $r'[0, r_f]$. The equation becomes

$$r k_f \frac{dT_f}{dr}\bigg|_0^{r'} + \frac{r q'''}{2}\bigg|_0^{r'} = 0 \tag{3.51}$$

The fuel centerline temperature $T_f(0)$ is required to be finite

$$\frac{dT_f}{dr}\bigg|_{r=0} < \infty \tag{3.52}$$

the equation reduces to

$$r' k_f \frac{dT_f(r')}{dr} + \frac{r' q'''}{2} = 0 \tag{3.53}$$

Dividing the equation by r' and integrating the equation over $r' \in [0, r]$

$$\int_0^r k_f \frac{d\,T_f(r')}{d\,r} d\,r' + \int_0 r \frac{r' q'''}{2} = 0 \tag{3.54}$$

$$k_f \left(T_f(r) - T_f(0)\right) + \left.\frac{(r')^2 q'''}{4}\right|_0^r = 0 \tag{3.55}$$

$$\left(T_f(r) - T_f(0)\right) + \frac{r^2 q'''}{4k_f} = 0 \tag{3.56}$$

Rearranging the equation

$$T_f(0) = T_f(r) + \frac{r^2 q'''}{4k_f} \tag{3.57}$$

At $r = r_f$

$$T_f(0) = T_f(r_f) + \frac{r_f^2 q'''}{4k_f} \tag{3.58}$$

The volumetric heat generation can be related to the linear power density as

$$q''' = \frac{q'}{\pi r^2} \tag{3.59}$$

Substituting this in equation Eq. 3.57

$$T_f(0) = T_f(r_f) + \frac{q'}{4\pi k_f} \tag{3.60}$$

Thus, the coolant, cladding outer surface and fuel centerline temperatures are calculated at each axial level. The sample is rejected if any of the components temperatures exceeds the temperature constraints for the design.

3.3.5 Input/Output Processing

The thermal hydraulic screening function results in a judgment whether a design sample is accepted or rejected based on the compliance with the thermal hydraulic constraints. For accepted samples, a multiphysics analysis is performed on them. The analysis includes coupled neutronics, thermal hydraulics and thermal expansion simulation. Additionally, a depletion analysis is carried out for each of them. As described earlier, `LUPINE` code is a LMFR simulator which can perform a coupled multiphysics simulation. The code was adopted in the application of DOM presented in this project. The procedure of creating a `LUPINE` model was presented in Fig. 2.3

The preparation of the `LUPINE` model for a design sample comprises four stages. At first, the smeared material number densities are calculated using `HEXBLD`. The Python program prepares an input file for each fuel assembly type in a design sample and calls `HEXBLD` to run them. `HEXBLD` input requires defining the fuel assembly radial dimensions, number of fuel pins in the assembly

N_{pins}, fuel material, cladding material, fuel pin dimensions, the coolant type, nature of the gas gap region (gas gap or bond), N-15 enrichment (when UN fuel is used), and fuel porosity.

The fuel assembly pitch P_{Assembly} is selected via the sampling function. The dimensions required for `HEXBLD` input are calculated based on the description of the fuel assembly components as presented in Eq. 3.7. Based on the calculation of the geometry function, the number of fuel pins per assembly is passed to the function that writes `HEXBLD` inputs. The radius of the fuel pin is borrowed from the results of the sampling function, too. The clad thickness is calculated based on the Clad Thickness Ratio (CTR) which is defined as

$$\text{CTR} = \frac{t_{clad}}{2R} \tag{3.61}$$

where R is the fuel pin radius. The CTR is required to be entered by the user in the input file. The CTR was set to a constant value (The value calculated for WEC long-life core LFR fuel pin design) for all design samples and this value is

$$\text{CTR} = 0.05358 \tag{3.62}$$

The Python program calculates the clad thickness for each case that passes the thermal hydraulic screening based on CTR.

The gap region thickness was set to be constant (As calculated for the original design) through all the design samples

$$t_{gap}\,[\text{cm}] = 5.13 \times 10^{-3} \tag{3.63}$$

Once the `HEXBLD` input files are ready for a design sample, `HEXBLD` code is executed and the number densities are passed to `LUPINE` input file.

The second stage in preparing the `LUPINE` model is building the mesh. `HEXCORE` was used for generating the mesh file in this work. The code accepts input file in a DIF3D input format. For each accepted design sample, the Python program writes the core model in DIF3D input format and executes `HEXCORE` to generate the mesh in VTK format. The mesh is finally passed to `LUPINE` input of the particular case.

The third stage in modeling a design sample in `LUPINE` is providing the cross section library. MC^2-3 is the code used in this project to generate multigroup cross sections for LMFR calculations. The process of generating cross sections for each design sample is computationally expensive. To save computational power and time, it was assumed that the microscopic cross sections generated by MC^2-3 are constant (i.e. independent of the geometry). This assumption needs to be tested. Therefore, a test to examine the sensitivity of design samples to the cross section libraries has been performed. In this test, two design samples were selected randomly. Cross section libraries were generated for each one using MC^2-3. Each case was run with `LUPINE` based on its own cross section library. After that, the library generated for the first case was fed to the second case. The effect of the cross section library was quantified to be less than 100pcm.

Based on this discussion, one cross section library was generated and used for all design sam-

ples generated by the Python program. The library consists of four sub-libraries. Each sub-library contains cross-sections at a unique set of component temperatures.

In the fourth stage of preparing the LUPINE model, LUPINE input is written for each accepted design sample. The number densities, mesh file and cross section library are fed to the LUPINE input file. The design sample is also prepared to perform depletion calculations. Lastly, each design sample is run using LUPINE.

3.3.6 Economic Analysis

Once LUPINE finishes running the cases, the depletion results are obtained from the output files. The cycle length, and inner core, middle core and outer core enrichments are passed to the economic analysis function. The function assumes a fresh core with three enrichment zones. To evaluate the fuel cycle cost, the LCOE was used. Details of the fuel cycle cost calculations can be found in Appendix A. The costs of the fuel cycle stages are provided in Table 3.1 The assumed rates used in

Table 3.1 Assumed Fuel Cycle Component Costs [Kim19]

Cost type	Unit	Value
ore cost	\$/lb	40
conversion cost	\$/kg	10
SWU cost	\$/kg	70
fabrication cost	\$/kgU	500
Decontamination and dismantling (D&D) rate	\$/month	82494
disposal	\$/MW$_e$.hr	1

the fuel cycle calculations are shown in Table 3.2. It should be noted that these are typical values used in fuel cycle calculations.

3.3.7 Post-Processing

LUPINE output files for each case are read. The maximum component temperatures as a function of depletion time are obtained. These temperatures are then compared to the design constraints. Design samples which violate the design constraints are discarded from further processing. For the designs that pass this last filter, a cost function is calculated as follows

$$\text{Cost Function} = \text{LCOE} \tag{3.64}$$

which minimizes the cost of the fuel cycle. The design with the smallest cost function among the cases analyzed is considered to be the optimal design.

Table 3.2 Rates Used During the Fuel Cycle Calculation

item	unit	value
escalation rate	%	0
fabrication escalation rate	%	5
pre-operation carrying charges	%	6
carrying charges rate	%	2
property tax rate	%	0
conversion loss	%	0.5
fabrication loss	%	0.1
enrichment loss	%	0.5
feed enrichment	%	0.71
tails enrichment	%	0.25
conversion to enrichment time	days	60
enrichment to fabrication	days	60
Fabrication to startup	days	120
Capacity Factor	%	98

3.4 Summary

In this chapter, the general purpose design and optimization methodology called DOM has been detailed. The methodology is a search space investigation technique. The ultimate goal of DOM is to enable fast and efficient exploration of a search space. To demonstrate the usage of DOM, a nuclear core design application was used. This was the design and optimization of LMFRs. In this project, we specifically focused on LFRs. A Python program was written to automate the application of DOM to optimize the WEC long-life core LFR. The details of the program have been discussed.

CHAPTER

4

RESULTS

4.1 Introduction

LUPINE was originally developed to perform the multiphysics analysis of SFRs. The modeling and simulation capabilities to simulate LFRs were added to LUPINE in this project. To test these new capabilities, the first part of this chapter presents a case study based on the WEC long-life core LFR design [Kim19]. The multiphysics analysis of this design was carried out. A quantification of the contribution of individual physics was performed and the results have been presented. Additionally, a depletion analysis for the core has been done and the results have been presented. Finally, the fuel cycle cost for the design was also calculated.

DOM has been developed as a general purpose design and optimization methodology that aims to efficiently explore a search space. Of special interest to this project is to apply this methodology to a reactor core design. In the second part of this chapter, the methodology was applied to optimize the WEC long-life core LFR. The definition of the domain of the search space, and reactor objectives and constraints are presented. The design proposed by DOM as an optimized design will also be presented and analyzed.

4.2 WEC Long-Life Core LFR LUPINE model

WEC long-life core LFR is a 950 MW_{th} pool-type lead-cooled reactor fueled by UN. The goal of this design is to achieve a long fuel cycle. The decision to fuel this reactor with UN was based on the fact that it is the best performing fuel that allows for long fuel cycle length and reduced cycle cost [Kim19]. It also stems from the fact that UN fuel has better thermo-mechanical properties compared

to other types of fuel. The WEC long-life core LFR uses the double stabilized austenitic steel (DS4) as a structural material. DS4 is a promising structural material for LMFR technology for its low swelling behavior and corrosion resistance.

The long-life core LFR was designed by WEC based on two objectives. These are maximizing burnup and minimizing the change in core multiplication factor over the depletion cycle. The general characteristics of the reactor and its geometry are presented in Table 4.1. The specifications of the fuel assembly design are presented in Table 4.2. A radial mid-plane view of the reactor core is shown in Fig. 4.1. The figure shows the inner core (IC), middle core (MC), outer core (OC), reflector (REF) and shield (RSH) assembly locations in the core hexagonal grid. The locations with symbol EMP refer to the control and safety rod locations in the core. These locations are left filled with lead coolant through all of the calculations presented in this chapter (No control material considered in the design).

Table 4.1 WEC Long-life Core LFR General Reactor Specifications [Kim19].

Parameter	Value
Core Power [MW_{th}]	950
Structural and Cladding material	DS4
Total number of assembly locations	451
Number of fuel assemblies	289
Active Fuel Height [cm]	220.0
Coolant inlet temperature [K]	693.15
Number of core enrichment regions	3
Cycle length [EFPY]	25
Average Coolant Velocity $\left[\frac{m}{s}\right]$	1.49

The core utilizes UN fuel with natural nitrogen enrichment. The fuel design specifications are presented in Table 4.3. The fuel pin design description in [Kim19] was used in an attempt to calculate the masses of the heavy metals in the core. The absence of essential material properties and detailed description of the fuel pin design made it difficult to reproduce the masses presented for the original design in [Kim19]. Therefore, the calculated masses presented in this work are not in exact agreement with the masses presented for the original design. It should be noted, however, that the mass differences were fairly small. For the total core ^{235}U mass, the difference was less than 0.0138[%]. For the total core ^{238}U mass, the difference was less than 0.1298[%]. The heavy metal masses as calculated by our tools are presented in Table 4.4. For comparison, the masses presented by the original design can be found in [Kim19].

Table 4.2 WEC Long-life Core LFR Assembly Design Parameters [Kim19].

Parameter	Value
Assembly Pitch [cm]	16.3
Inter-assembly gap [cm]	0.4
Assembly duct thickness [cm]	0.35
Number of fuel pins per assembly	61
CTR	0.0535
Fuel pellet radius [cm] [1]	0.7524
cladding inner radius [cm] [1]	0.75756
Fuel pin radius [cm] [1]	0.8485
Pitch-Diameter ratio	1.143

[1] These values were based on internal communication with F. Franceschini. The fuel pin radius is different from the value provided in [Kim19].

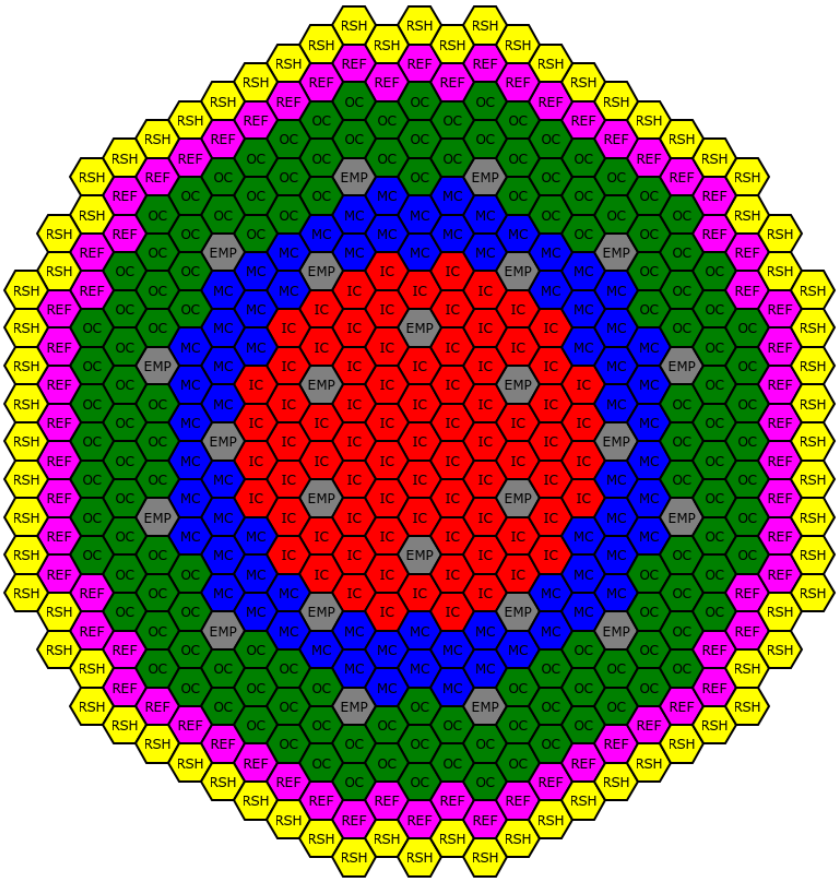

Figure 4.1 Mid-plane view of the WEC long-life core LFR core.

Table 4.3 WEC Long-life Core LFR Fuel Pin Design Specifications [Kim19].

Parameter	Value
Fuel Type	UN
Fuel porosity [%]	15
Nitrogen-15 enrichment [%]	0.4
Inner core enrichment [%]	10.3
Middle core enrichment [%]	11.8
Outer core enrichment [%]	13.8

Table 4.4 BOC Heavy Metal Masses.

Region	U-235 mass [kg]	U-238 mass [kg]
Inner Core	2217.90	19315.18
Middle Core	2315.73	17309.15
Outer Core	5190.71	32423.13

4.3 Multiphysics Simulation Results

The capabilities to simulate LFRs in `LUPINE` have been applied to the WEC long-life core LFR. A model of the reactor has been created for `LUPINE`. Fig. 4.2 shows the materials distribution in the reactor. The neutronics solver was based on the Simplified P_3 (SP_3) approximation. Three simulations were run to demonstrate the multiphysics feedback. The first is a Hot Zero Power (HZP) without thermal expansion. In this case the thermal power is set to zero and no thermal expansion treatment is considered. In other words, both the thermal expansion and thermal hydraulic feedback are turned off. The cross section library for this case was generated using MC^2-3 at coolant core inlet temperature (i.e. 693.15 [K]). In the second, a HZP with thermal expansion case was run. In this case, the thermal power is set to zero and the reactor materials were expanded at coolant inlet temperature (i.e. the thermal expansion is turned on while the thermal hydraulic feedback is off). The cross section library for this case was generated at the coolant core inlet temperature, too.

In the last simulation, the Hot Full Power (HFP) core was modeled. In this case, the thermal hydraulic and thermal expansion are both turned on. A temperature dependent cross section library was generated for the HFP case. The cross section library contained four sublibraries. Each sublibrary was generated at a unique set of fuel, gap, clad and coolant composition temperatures. The goal is to cover component operational temperatures by the temperature boundaries available in the cross section sublibraries. Based on the temperature of a composition, the cross sections are determined by interpolating between the cross section sublibraries. The interpolation for the fuel composition is based on a square root interpolation in order to capture the Doppler effect. The results of the multiphysics analysis are shown in Table 4.5.

The worth of the thermal expansion and thermal hydraulic feedback together is −575.5 [pcm]

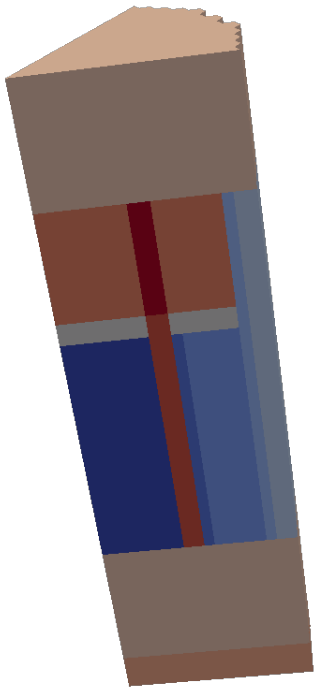

Figure 4.2 Materials of WEC long-life core LFR

Table 4.5 Multiphysics `LUPINE` Calculated Eigenvalues for WEC Long-life Core LFR

Case	TE[1] power	TH[2] power	Eigenvalue
HZP no TE	0%	0%	1.026104
HZP	100%	0%	1.022118
HFP	100%	100%	1.020080

[1] TE: Thermal Expansion
[2] TH: Thermal Hydraulic

[1]. Of this, −380.1 [pcm] are attributed to the thermal expansion. The worth of thermal hydraulic feedback is −195.5 [pcm]. These were calculated based on

$$\begin{aligned} d\rho &= \rho_1 - \rho_2 \\ &= \frac{k_{\text{eff},1}-1}{k_{\text{eff},1}} - \frac{k_{\text{eff},1}-1}{k_{\text{eff},1}} \\ &= \frac{k_{\text{eff},1}-k_{\text{eff},2}}{k_{\text{eff},1}k_{\text{eff},2}} \end{aligned} \tag{4.1}$$

[1] 1 pcm $= 10^{-5}\frac{dk}{k}$

4.4 Depletion

Based on the results presented in [Kim19], the WEC long-life core LFR effective cycle length is 25 [years]. Therefore, LUPINE was used to deplete the core for 25 years. Fig. 4.3 shows the multiplication factor as a function of time up to the cycle length. The End Of Cycle (EOC) heavy metal masses calculated by LUPINE are presented in Table 4.6.

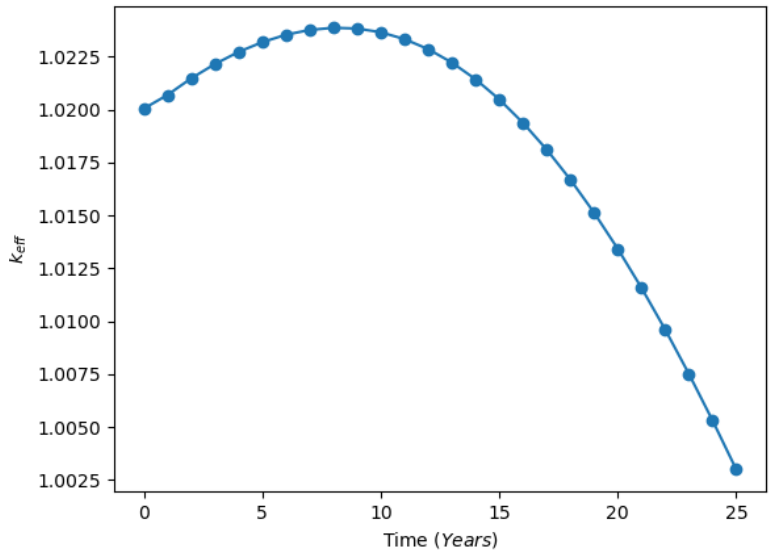

Figure 4.3 Multiplication factor as a function of reactor depletion time.

Table 4.6 EOC Heavy Metal Masses.

Element	U235	U236	U238	PU238	PU239	PU240	PU241	PU242	others
Mass [kg]	3675.546	1137.36	61275.60	35.77	4602.76	554.90	32.02	2.77	142.16

Based on the results presented in [Kim19], the EOC multiplication factor is 1.0. Based on the results obtained by LUPINE, the EOC multiplication factor at the end of year 25 is 1.00308. To account for this bias, the multiplication factor value 1.00308 is considered to be the critical eigenvalue. The EOC is considered to be reached if the multiplication factor of the core drops below this value.

The BOC and EOC reactor power distributions are shown in Fig. 4.4. The top view of the power distribution at active core region mid-plane is shown in Fig. 4.5. As can be seen, the power peaking in WEC long-life core LFR travels from near the core periphery towards the core center. This is due to the build up of ^{239}Pu in the core and migration of the depletion zone towards the core center.

The LCOE calculated using the economic analysis tool was 6.94 $\left[\frac{\$}{\mathrm{MW}_e.\mathrm{hr}}\right]$. The detailed economic analysis of the WEC long-life core LFR is presented in Appendix A (Section A.5). The LCOE for the design is calculated by Eq. A.67.

The reported LCOE in [Kim19] is 7.5 $\left[\frac{\$}{\mathrm{MW}_e.\mathrm{hr}}\right]$, which is higher than the LCOE calculated in this work. Differences might be due to the methodologies in accounting for LCOE. Details and an example for the calculation of the LCOE presented in Appendix A.

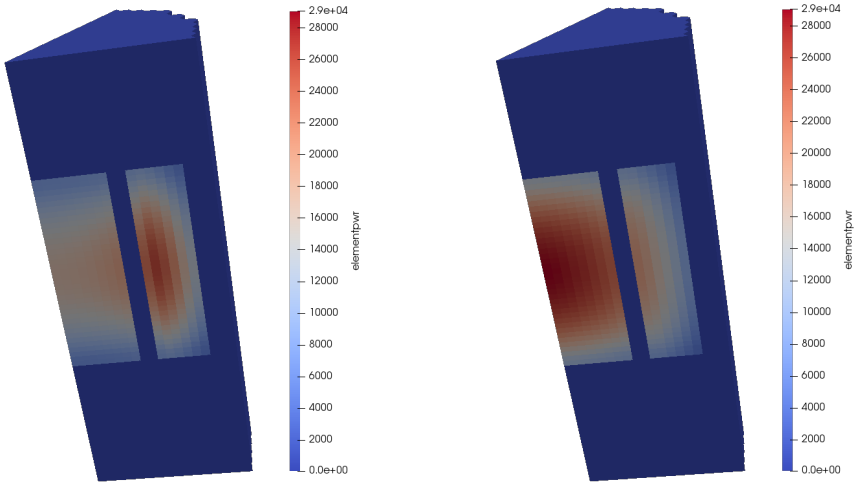

(a) **(b)**

Figure 4.4 WEC design: comparison of (a) BOC and (b) EOC core power distribution

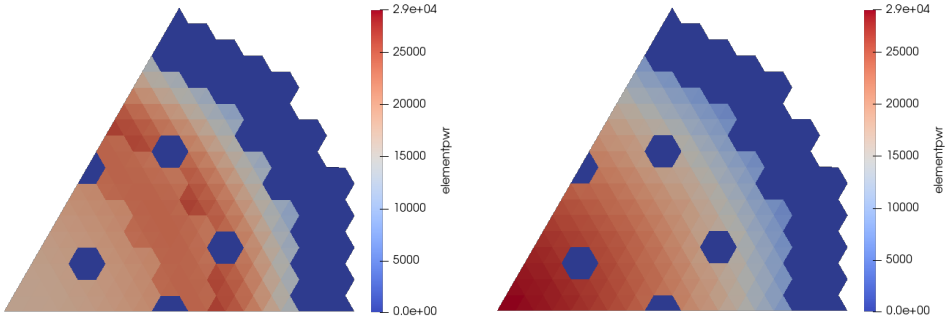

(a) **(b)**

Figure 4.5 WEC design: comparison of (a) BOC and (b) EOC active fuel region mid-plane power distribution

4.5 Reactivity Coefficients

The concept commonly used in nuclear reactor analysis to describe the state of the reactor relative to a critical state (i.e. $k_{\text{eff}} = 1$) is called reactivity (ρ). It can be mathematically described as

$$\rho = \frac{k_{\text{eff}} - 1}{k_{\text{eff}}} \tag{4.2}$$

Based on this, the reactivity of a reactor at a critical state is zero (i.e. $\rho = 0$). If a reactor is subcritical, then $k_{\text{eff}} < 1$ which results in a negative reactivity. When the reactor is supercritical, the reactivity is positive.

A reactivity coefficient in reactor analysis is a concept that describes the change in a reactor's reactivity relative to an infinitesimal change in a quantity of interest (x). The Reactivity coefficient of a quantity x at a value x_i can be mathematically described as

$$\alpha_x(x_i) = \left.\frac{\partial \rho}{\partial x}\right|_{x_i} \tag{4.3}$$

This can be approximated using a finite difference expression as

$$\begin{aligned} \alpha_x(x_i) &= \left.\frac{\Delta \rho}{\Delta x}\right|_{x_i} \\ \Rightarrow \alpha_x(x_i) &= \frac{\rho(x_i + \Delta x) - \rho(x_i)}{\Delta x} \end{aligned} \tag{4.4}$$

4.5.1 Power Reactivity Coefficient

The power reactivity coefficient can be defined as the change in reactivity due to a change in reactor power. The coefficient includes information about all individual reactivity effects in a reactor happening together. A stable reactor should have a negative power reactivity coefficient (i.e. $\alpha_{\text{power}} < 0$). This ensures that increasing the reactor power requires a reactivity insertion which results in preventing a runaway power increase. The power reactivity coefficient at a reactor power level P_{Rx} can be calculated as

$$\alpha_{\text{power}}(P_{\text{Rx}}) = \frac{\rho(P_{\text{Rx}} + \Delta P_{\text{Rx}}) - \rho(P_{\text{Rx}})}{\Delta P_{\text{Rx}}} \tag{4.5}$$

4.5.2 Thermal Expansion Reactivity Coefficient

In the case of positive reactivity insertion, the reactor power increases and the reactor component temperatures increase in response. As the temperature increases, the fuel and structural materials expand, resulting in a reduction of the reaction rate in reactor materials. This, in turn, increases the neutron leakage out of the core and, in response, reduces the reactivity. This is very important in maintaining LMFRs stability and ensures safety of reactor operation especially during reactivity initiated accidents. The thermal expansion reactivity coefficient is defined as the change in reactivity

due to a change in reactor dimensions taking place as a result of the thermal expansion of reactor components. At a reactor power level P_{Rx}, this coefficient can be calculated as

$$\alpha_{\text{thexp}}(P_{\text{Rx}}) = \frac{\rho(T_{\text{exp}}(P_{\text{Rx}} + \Delta P_{\text{Rx}})) - \rho(T_{\text{exp}}(P_{\text{Rx}}))}{\Delta P_{\text{Rx}}} \tag{4.6}$$

where $\rho(T_{\text{exp}}(P_{\text{Rx}}))$ is the reactivity at power level P_{Rx} with the reactor components thermally expanded to a temperature $T_{\text{exp}}(P_{\text{Rx}})$. $\rho(T_{\text{exp}}(P_{\text{Rx}} + \Delta P_{\text{Rx}}))$ is the reactivity calculated when the reactor components are further expanded due to a ΔP_{Rx} change in the reactor power.

4.5.3 Fuel Temperature Reactivity Coefficient

It is well known that neutron cross sections for heavy metals exhibit absorption resonances at certain energies. As the temperature of the fuel material increases, the thermal motion of the target nuclei increases resulting in a broadening of the cross section resonance. This effect is known as the Doppler broadening effect. The phenomena results in an increase of the absorption in the fuel material which introduces negative reactivity. The fuel temperature reactivity coefficient is defined as the change in reactor reactivity due to a change in fuel temperature. It can be calculated as

$$\alpha_{\text{Doppler}}(P_{\text{Rx}}) = \frac{\rho(T_{\text{fuel}} + \Delta T_{\text{fuel}}) - \rho(P_{\text{Rx}})}{\Delta T_{\text{fuel}}} \tag{4.7}$$

4.5.4 Coolant Temperature Coefficient

The coolant temperature coefficient is defined as the change in reactivity due to a change in the coolant temperature. With a reactivity insertion, the coolant temperature increases. As a result, two effects can be expected. The first is the increase of the coolant absorption cross section as a result of the Doppler broadening effect. The second is the reduction of the coolant density which results in a decreased neutron absorption rate in the coolant (i.e. more neutron availability for fast fission). Thus, it is expected that the coolant temperature coefficient will be positive in LMFRs. The coolant temperature reactivity coefficient can be mathematically defined as

$$\alpha_{\text{CTC}}(P_{\text{Rx}}) = \frac{\rho(T_{\text{cool}} + \Delta T_{\text{cool}}) - \rho(P_{\text{Rx}})}{\Delta T_{\text{cool}}} \tag{4.8}$$

The quantification of the coolant temperature coefficient is important to understand the stability of the reactor. Since it is expected to be positive for a LMFR, it must not be the dominant reactivity coefficient of a reactor.

4.5.5 Reactivity Coefficient Results

The `LUPINE` model of the WEC long-life core LFR was used to calculate the four reactivity coefficients discussed earlier. The reactivity coefficients were calculated as a function of reactor power level. The results are presented in Fig. 4.6

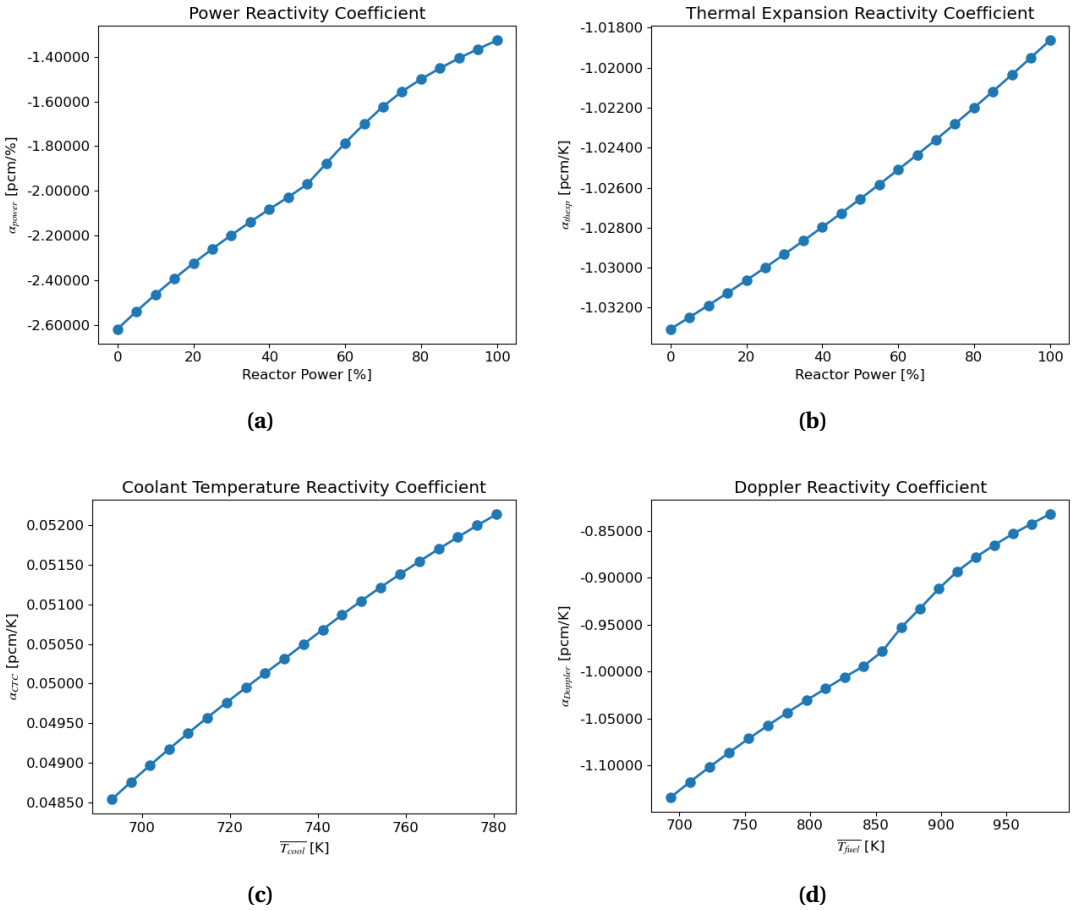

Figure 4.6 (a) Power (b) Thermal expansion (c) Coolant temperature and (d) Fuel temperature reactivity coefficients

As can be noticed in Fig. 4.6, the Doppler and thermal expansion reactivity coefficients are negative. These two reactivity coefficients dominate the positive coolant temperature coefficient. As a result, the power reactivity coefficient is negative which shows that the reactor is stable.

The negative sign of the thermal expansion coefficient can be explained by the reduction in density of reactor core components which leads to smaller reaction rates in the core. This, in turn, increases the neutron leakage component for the core. The coolant temperature coefficient is positive. Its value increases with increasing coolant temperature as expected. The Doppler reactivity coefficient exhibits a decrease in the value as the fuel temperature increases.

4.6 Optimization of WEC long-life core LFR

The second part of this chapter will apply DOM to the WEC core to attempt to modify the design and obtain a lower LCOE. DOM has been presented in Chapter 3 as a general purpose design and optimization method that is based on the effective exploration of a search space. In the following

subsections, the stages of the search space set up and the optimized design suggested by DOM for WEC long-life core LFR will be presented and analyzed. For more insights into the process of applying DOM to the WEC design, the reader is referred to Appendix B.

4.6.1 Objectives and Constraints

As discussed earlier, the first step in a design process is to identify the objectives of the design. Additionally, in order to address material limitation and assure the safe operation of the design, a set of constraints are set up, too. The objectives and constraints of the WEC long-life core LFR are presented in Table 4.7.

Table 4.7 WEC Long-life Core LFR Design Objectives and Constraints [Kim19]

Parameter	Value
Lead coolant velocity $\left[\frac{m}{s}\right]$	< 2 (Soft constraint)
Fuel maximum temperature [K]	1773.15
Maximum Cladding temperature [K]	1085.15
Maximum enrichment [%]	< 19.9
Active Core length [m]	< 3
Target cycle length [years]	10-30
Inter-assembly gap [cm]	0.4

An additional constraint to those presented in the table is that the core should fit within a barrel of 3.9 [m] diameter. This can lead to a higher active fuel height. The WEC long-life LFR core uses the novel concept of common-plenum fuel assembly design [Kim19]. This allows for increasing the active fuel height without resulting in an increase in the reactor barrel height. Finally, it should be noted that the inter-assembly gap of 0.4 [cm] was used for all samples generated in the application of DOM. This value was used to account for the duct bowing and swelling [Kim19].

4.6.2 Domain of Search Space

The parameters constituting the search space were suggested to be fuel pin radius, P/D ratio, assembly pitch, fuel height, inner core enrichment and outer core enrichment. The identification of the domain of the search space was made based on a literature review combined with performing computer experiments to understand the sensitivity of the design to the parameters. The domain of the search space is presented in Table 4.8. It should be noted that the selection of the lower limit of P/D in the domain was governed by the fact that the Nusselt number (Nu) correlation range of applicability doesn't cover P/D smaller than a value of 1.1. Additionally, the upper limit of the fuel assembly pitch was set up according to the constraint that the reactor should fit inside a reactor barrel of a diameter of 3.9 [m] [Kim19]. Finally, it should be noted that the coolant velocity was set

up to 1.8 $\left[\frac{m}{s}\right]$ for all generated samples.

Table 4.8 Definition of the Domain of the Search Space

Explanatory variable	Range
Pin radius [cm]	[0.6, 0.9]
Pitch-to-Diameter ratio	[1.1, 1.3]
Assembly pitch [cm]	[16.1, 16.3]
Fuel height [cm]	[200, 350]
Inner core enrichment [%]	[7.21, 11]
Middle core enrichment[%]	[11, 12]

4.6.3 Results of the Optimization

As mentioned earlier in the thesis, a Python program was used to automate the application of DOM. Based on the domain of the search space, 1500 samples were requested from the Python LHS sampling module. Of them, 34.5 [%] (518 samples) passed the thermal hydraulic screening. For each of these successful cases, `LUPINE` was used to run a multiphysics simulation and to perform a core depletion. The end of cycle is considered to be reached once the core multiplication factor drops below the value of the critical eigenvalue discussed earlier (i.e. $k_{\text{eff}} = 1.00308$). The optimization goal was to reduce the LCOE. DOM eventually suggested the fuel assembly design presented in Table 4.9. DOM suggested enrichment distribution in the core as presented in Table 4.10.

Table 4.9 Specifications of Assembly Design for the Optimized Core

Parameter	Optimized Core Value	Original Design
Assembly pitch [cm]	16.25	16.3
Inter-assembly gap [cm]	0.4	0.4
Assembly duct thickness [cm]	0.3491	0.35
Number of fuel pins per assembly	61	61
Fuel pellet radius [cm]	0.7594	0.7524
Cladding inner radius [cm]	0.7646	0.75756
Fuel pin radius [cm]	0.8564	0.8485
Active Fuel height [cm]	220	220

A depletion analysis was performed using `LUPINE`. The core showed that it can sustain criticality for 27.5 [years]. The multiplication factor of the core as a function of depletion time is shown in Fig. 4.7. The LCOE for the optimum reactor was calculated to be 6.76 $\left[\frac{\$}{\text{MW}_e.\text{hr}}\right]$ which represents 2.56[%] reduction in fuel cycle cost.

Table 4.10 Optimized Core Fuel Enrichment Distribution

Value	Optimized Core Value	Original Design
Inner core enrichment [%]	10.08	10.3
Middle core enrichment [%]	11.26	11.8
Outer core enrichment [%]	14.55	13.8

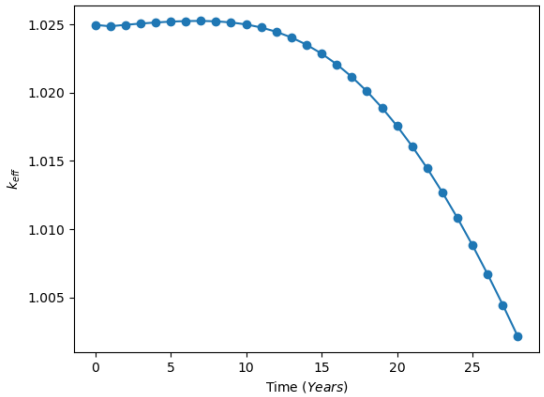

Figure 4.7 The optimized design multiplication factor as a function of depletion time

4.6.4 Multiphysics Results

The optimum core multiphysics has been tested with `LUPINE`. Three tests were performed. These were the HZP without thermal expansion, HZP with thermal expansion and HFP. The results are shown in Table 4.11.

Table 4.11 Multiphysics `LUPINE` Calculated Eigenvalues for optimized WEC Long-life Core LFR

Case	TE[1] power	TH[2] power	Eigenvalue
HZP no TE	0%	0%	1.031028
HZP	100%	0%	1.026745
HFP	100%	100%	1.024978

[1] TE: Thermal Expansion
[2] TH: Thermal Hydraulic

Based on these results, the thermal expansion and thermal hydraulic feedback account for −572.5 [pcm]. −404.6 [pcm] is attributed to thermal expansion. The rest (i.e. −167.9 [pcm]) are due to thermal hydraulic feedback.

The BOC and EOC power distribution of the optimized core are shown Fig. 4.8. The BOC and EOC active fuel region mid-plane power distributions are shown in Fig. 4.9

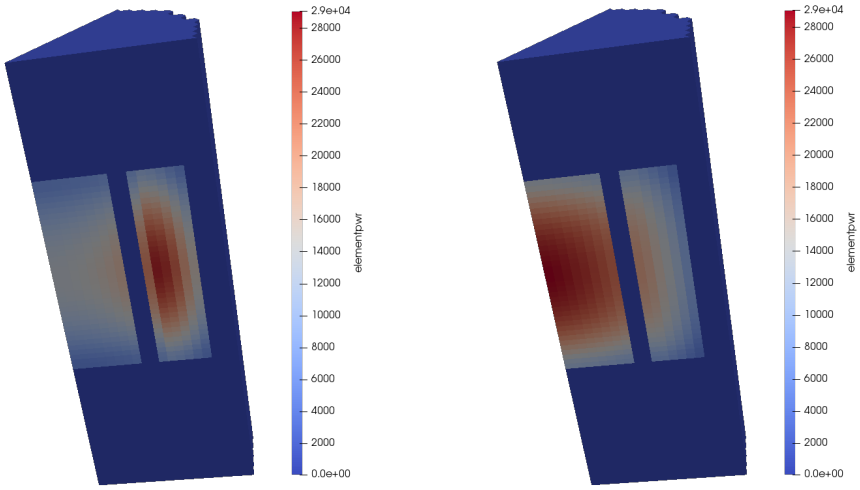

(a) **(b)**

Figure 4.8 Optimized design: comparison of (a) BOC and (b) EOC core power distribution

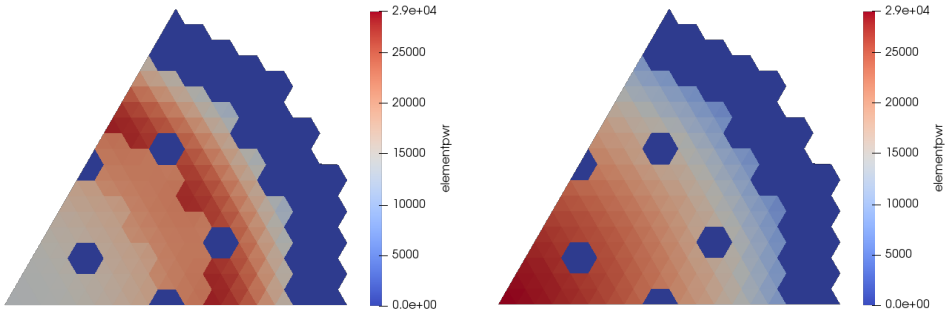

(a) **(b)**

Figure 4.9 Optimized design: comparison of (a) BOC and (b) EOC core power distribution

The reactivity coefficients were calculated for this optimized design, too. The results are shown in Fig. 4.10. The power reactivity coefficient of the design is negative which makes the reactor stable. The coolant temperature reactivity coefficient is positive (as expected). It is smaller in magnitude than the coolant temperature coefficient of the original design. The thermal expansion and Doppler reactivity coefficients have similar trends to those calculated for the original design. However, the thermal expansion coefficient is less negative than that for the original design while the Doppler coefficient is quite similar.

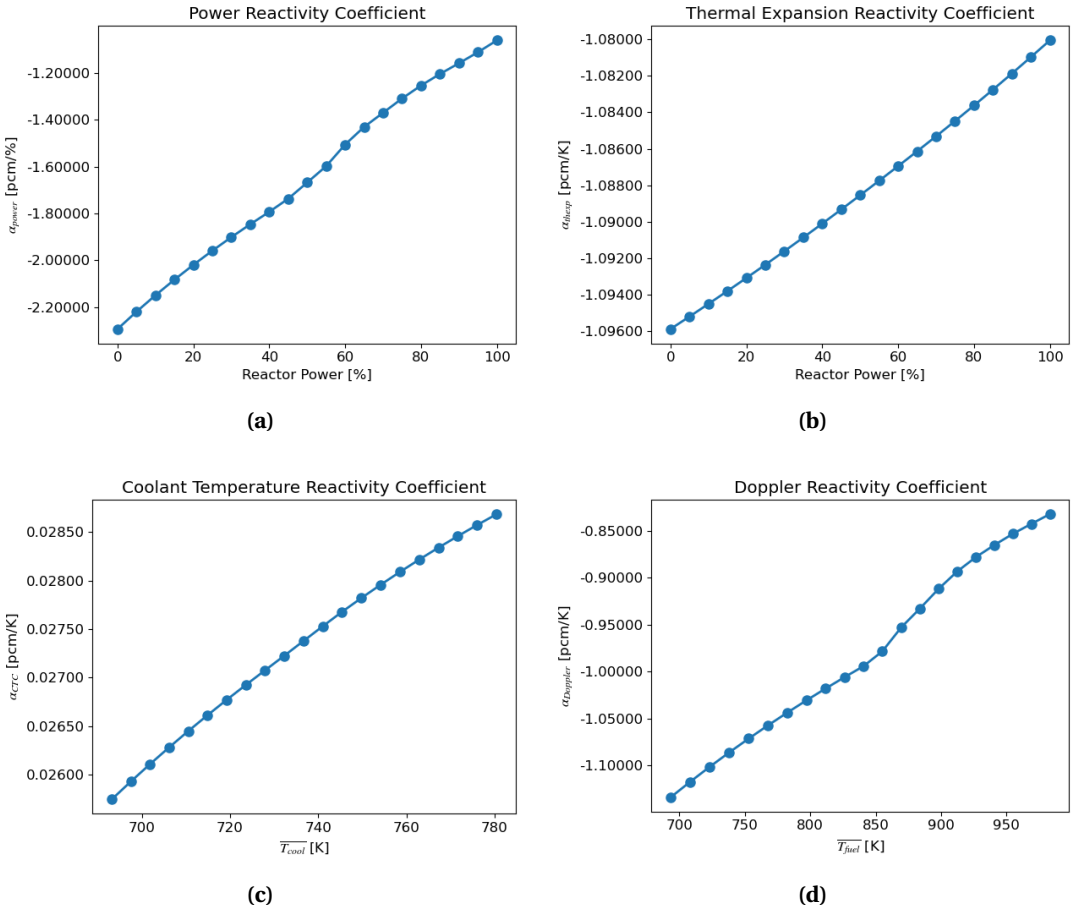

Figure 4.10 (a) Power (b) Thermal expansion (c) Coolant temperature and (d) Fuel temperature reactivity coefficients of the optimized design

4.7 Summary

In this chapter, the capabilities to model LFRs using `LUPINE` have been tested. The models have been applied to the WEC long-life core LFR. The results of the multiphysics simulation were presented in addition to the reactivity coefficients calculation.

DOM has been used to optimize the core. The goal was to reduce the LCOE of the core. As a result, a 2.62 [%] reduction on the LCOE has been achieved. A depletion, reactivity coefficient and multiphysics analysis has been carried out for the optimized design. These results have been presented and compared to the original core design.

CHAPTER

5

CONCLUSIONS AND FUTURE WORK

There has been a growing interest in LMFR reactor technology in the last two decades. Plans are underway to commercialize the technology. The history of LMFRs goes back to the beginning of the nuclear power generation. The Experimental Breeder Reactor I (EBR-I), for example, was the first power reactor to generate electricity in 1951.

Although SFRs have attracted the most attention in the community, a significant experience has been gained with LFRs, too. The features of the lead coolant makes LFRs a favorable technology. At the same time, the LFR technology is facing some material limitation challenges. Newly developed materials are being investigated and developed to address such challenges.

The modeling and simulation capabilities of LMFRs are not as mature as those of LWRs. At North Carolina State University, `LUPINE` computer code was developed to enable the modeling and simulation of LMFRs. Originally, `LUPINE` was developed for the modeling and simulation of SFRs. The addition of LFRs modeling and simulation capabilities was the first part of this thesis. The improvements on `LUPINE` included neutronic and thermal models of lead coolant, UN thermal conduction and thermal expansion models, gas gap region conduction model and core mass flow distribution. These new capabilities have been tested using the WEC long-life core LFR.

There have been very few papers in the literature describing the optimization of LMFR reactor core design. In the second part of the thesis, the DOM has been proposed as a general purpose methodology. The theory of DOM has been presented in this thesis. The methodology has been applied to optimize the WEC long-life core LFR. A Python program was written to automate this application. The theory behind this program has been presented. The goal of the optimization was to reduce the LCOE. A reduction of 2.56[%] on the LCOE has been achieved. This corresponds to a cost savings of almost 18M [$] over the life of the reactor.

5.1 Future Work

DOM is a general purpose design and optimization methodology. In this work, the application of the DOM has been focused on LFRs with UN fuel. A Python program was written to apply DOM. Extending the Python program to include other liquid metal coolants, reactor materials and fuels is a straightforward process.

The simulation and analysis in the application of the DOM to WEC long-life core LFR has involved neutronics, thermal hydraulics and economic analyses. Involving a structural mechanics analysis module in the decision making process can potentially make the converged optimum core more accurate. However, the biggest challenge that faces this step is the lack and/or accuracy of data and correlations presented in literature.

In the application of DOM presented in this work for the WEC LFR core, the considered constraints were limited to the material temperature limits, coolant velocity (to prevent erosion), and degree of fuel enrichment. In a more detailed scenario, the pressure drop of the coolant in the channel, fuel exposure, fission gas buildup, and possibly other constraints would be taken into account. It should be noted that adding more constraints to the optimization process is straightforward.

The WEC long-life core LFR design had locations to accommodate control and safety rods in its core. The design presentation in [Kim19] did not provide the description of the control elements. Had the control rod design been given and taking into account the criticality search capability currently being developed in `LUPINE`, a potential future work would be the modeling of the control rods and performing a search for the optimized core while performing a criticality search associated with the depletion calculations.

BIBLIOGRAPHY

[Ada21] Adamov, E. O. et al. “Brest Lead-Cooled Fast Reactor: From Concept to Technological Implementation”. *Atomic Energy* (2021).

[AD21] Al-Dawood, K. et al. “Multiphysics Simulation of Uranium-Nitride Fueled Lead-cooled Fast Reactor”. *Proceedings of M&C 2021*. 2021.

[Ale11] Alemberti, A. et al. “European lead fast reactorâĂŤELSY”. *Nuclear Engineering and Design* **241**.9 (2011). Seventh European Commission conference on Euratom research and training in reactor systems (Fission Safety 2009), pp. 3470–3480.

[Ale14] Alemberti, A. et al. “Overview of lead-cooled fast reactor activities”. *Progress in Nuclear Energy* **77** (2014), pp. 300–307.

[Bab09] Babazadeh, D. et al. “Optimization of fuel core loading pattern design in a VVER nuclear power reactors using Particle Swarm Optimization (PSO)”. *Annals of Nuclear Energy* **36**.7 (2009), pp. 923–930.

[Bre] *Construction licence issued for Russia’s BREST reactor*. URL: https://world-nuclear-news.org/Articles/Construction-licence-issued-for-Russias-BREST-reac#:~:text=A%20licence%20has%20been%20issued,lead%2Dcooled%20fast%20neutron%20reactor..

[Daw19] Dawn, W. C. “Simulation of Fast Reactors with the Finite Element Method and Multiphysics Models”. MS. North Carolina State University, 2019.

[DP20] Dawn, W. C. & Palmtag, S. “A Multiphysics Simulation Suite for Sodium Cooled Fast Reactors”. *Proceedings of PHYSOR 2020*. Cambridge, UK, 2020.

[DP21] Dawn, W. C. & Palmtag, S. “A multiphysics simulation suite for liquid metal-cooled fast reactors”. *Annals of Nuclear Energy* **159** (2021), p. 108213.

[DF95] DeChaine, M. D. & Feltus, M. A. “Nuclear Fuel Management Optimization Using Genetic Algorithms”. *Nuclear Technology* **111**.1 (1995), pp. 109–114.

[DD12] Deutsch, J. L. & Deutsch, C. V. “Latin hypercube sampling with multidimensional uniformity”. *Journal of Statistical Planning and Inference* **142**.3 (2012), pp. 763–772.

[Ekb18] Ekberg, C. et al. “Nitride fuel for Gen IV nuclear power systems”. *Journal of Radioanalytical and Nuclear Chemistry* **318** (2018), pp. 1713–1725.

[Fra03] FranÃğois, J. et al. “A practical optimization procedure for radial BWR fuel lattice design using tabu search with a multiobjective function”. *Annals of Nuclear Energy* **30** (2003), pp. 1213–1229.

[Gen] *Generation Four International Forum*. URL: https://www.gen-4.org/gif/.

[Gra14] Grasso, G. et al. “The core design of ALFRED, a demonstrator for the European lead-cooled reactors”. *Nuclear Engineering and Design* **278** (2014), pp. 287–301.

[Han] *Handbook on Lead-bismuth Eutectic Alloy and Lead Properties, Materials Compatibility, Thermal-hydraulics and Technologies*. Tech. rep. NEA–7268. Nuclear Energy Agency of the OECD (NEA), 2015.

[Hay90] Hayes, S. L. et al. “Material Property Correlations for Uranium Mononitride: I. Physical Properties”. *Journal of Nuclear Materials* **171** (1990), pp. 262–270.

[Hwa07] Hwang, I. S. *A sustainable regional waste transmutation system: PEACER*. Tech. rep. IAEA-tm-28911 TWG-FR/130. 2007.

[Kim18] Kim, T. et al. *Research and development roadmaps for liquid metal cooled fast reactors - draft for public comments*. Tech. rep. ANL/ART-88 Rev. 02. Argonne National Laboratory, 2018, pp. 73–81.

[Kim19] Kim, T. K. et al. “Long Core Life Design Options For The Westinghouse LFR”. *International Nuclear Fuel Cycle Conference (GLOBAL)*. Seattle, WA, 2019.

[KT91] Kropaczek, D. J. & Turinsky, P. J. “In-Core Nuclear Fuel Management Optimization for Pressurized Water Reactors Utilizing Simulated Annealing”. *Nuclear Technology* **95**.1 (1991), pp. 9–32.

[LY13] Lee, C. H. & Yang, W. S. *MC2-3: Multigroup Cross Section Generation Code for Fast Reactor Analysis*. Tech. rep. ANL/NE-11-41 Rev. 2. Argonne National Laboratory, 2013.

[Luo20] Luo, X. et al. “Automated core design code development for a lead-cooled fast reactor and its core optimization”. *International Journal of Energy Research* **n/a**.n/a (2020).

[Mck79] Mckay, M. et al. “A Comparison of Three Methods for Selecting Vales of Input Variables in the Analysis of Output From a Computer Code”. *Technometrics* **21** (1979), pp. 239–245.

[Mik09] Mikityuk, K. “Heat transfer to liquid metal: Review of data and correlations for tube bundles”. *Nuclear Engineering and Design* **239**.4 (2009), pp. 680–687.

[Moz20] Moza, S. *sahilm89/lhsmdu: Latin Hypercube Sampling with Multi-Dimensional Uniformity (LHSMDU): Speed Boost minor compatibility fixes*. Version 1.1.1. 2020.

[Pal21] Palmtag, S. et al. “Fast Reactor Depletion Methods In LUPINE”. *Proceedings of M&C 2021*. 2021.

[PS07] Pfrang, W. & Struwe, D. *Assessment of Correlations for Heat Transfer to the Coolant for Heavy Liquid Metal Cooled Core Designs*. Tech. rep. FZKA 7352. Karlsruhe: Forschungszentrum Karlsruhe GmbH, 2007.

[Pio16] Pioro, I. L., ed. *Handbook of Generation IV Nuclear Reactors*. Woodhead Publishing, 2016.

[Puk13] Pukari, M. “Experimental and Theoretical Studies of Nitride Fuels”. PhD dissertation. Royal Institute of Technology, 2013.

[QG14] Qvist, S. & Greenspan, E. “The ADOPT code for automated fast reactor core design”. *Annals of Nuclear Energy* **71** (2014), pp. 23–36.

[Roe19] Roelofs, F., ed. *Thermal Hydraulics Aspects of Liquid Metal Cooled Nuclear Reactors*. Woodhead Publishing, 2019.

[Rog03] Rogozkin, B. et al. “Mononitride Fuel for Fast Reactors”. *Atomic Energy* **95** (2003), pp. 624–636.

[San03] Santner, T. et al. *The Design and Analysis of Computer Experiments*. Springer, 2003.

[SY08] Sekimoto, H. & Yan, M. “Design study on small CANDLE reactor”. *Energy Conversion and Management* **49**.7 (2008). ICENESâĂŹ2007, 13th International Conference on Emerging Nuclear Energy Systems, June 3âĂŞ8, 2007, Äřstanbul, Turkiye, pp. 1868–1872.

[Sek01] Sekimoto, H. et al. “CANDLE: The New Burnup Strategy”. *Nuclear Science and Engineering* **139**.3 (2001), pp. 306–317.

[Sie08] Sienicki, J. et al. *Status report on the Small Secure Transportable Autonomous Reactor (SSTAR)/Lead-cooled Fast Reactor (LFR) and supporting research and development.* Tech. rep. Argonne National Lab.(ANL), Argonne, IL (United States), 2008.

[Sob11] Sobolev, V. *Database of thermophysical properties of liquid metal coolants for GEN-IV*. Tech. rep. SCK-CEN-BLG-1069. Belgian Nuclear Research Centre SCK-CEN, 2011.

[Sob12] Sobolev, V. “2.14 - Properties of Liquid Metal Coolants”. *Comprehensive Nuclear Materials*. Ed. by Konings, R. J. Oxford: Elsevier, 2012, pp. 373–392.

[SL17] SÃľran, J.-L. & Le Flem, M. “8 - Irradiation-resistant austenitic steels as core materials for Generation IV nuclear reactors”. *Structural Materials for Generation IV Nuclear Reactors*. Ed. by Yvon, P. Woodhead Publishing, 2017, pp. 285–328.

[Tuc06] Tucek, K. et al. “Comparison of sodium and lead-cooled fast reactors regarding reactor physics aspects, severe safety and economical issues”. *Nuclear Engineering and Design* **236**.14 (2006). 13th International Conference on Nuclear Energy, pp. 1589–1598.

[Wu16] Wu, Y. et al. “Development strategy and conceptual design of China Lead-based Research Reactor”. *Annals of Nuclear Energy* **87** (2016), pp. 511–516.

[YO19] Yoshiaki Oka Haruki Madarame, M. U., ed. *Fast Reactors System Design*. Springer, 2019.

[Zha13] Zhang, J. “Oxygen control technology in applications of liquid lead and leadâĂŞbismuth systems for mitigating materials corrosion”. *Journal of Applied Electrochemistry* (2013).

APPENDICES

APPENDIX

A

FUEL CYCLE CALCULATION

A.1 Introduction

In this appendix, the fuel cycle economic calculations are presented. These calculations have been used in this project to calculate the LCOE of the WEC long-life core LFR. A single-batch fuel cycle was considered (i.e. the calculation considered the BOC core loaded with fresh fuel). For the special case of the WEC long-life core LFR, there are three enrichment zones (i.e. inner core, middle core and outer core). In order to consider the different enrichments in the core, each enrichment zone is treated separately in the fuel cycle cost analysis.

A.2 Fuel Cycle Background

In a once-though fuel cycle, the front-end of the fuel cycle is composed of four conventional steps. These are mining, conversion, enrichment and fabrication. A quick overview of these four steps is as follows.

Uranium exists in earth's crust. ^{235}U represents about 0.71 [%] of the total naturally existing uranium. The rest is composed of ^{238}U and traces of ^{234}U. In the mining process, the ore is extracted from earth crust and chemically treated and purified. In the last stage of the mining process, U_3O_8 is produced in the form of a powder called "Yellow Cake" (also called "ore").

After mining, the ore must be converted to a form that can be used in enrichment. This is done by converting the U_3O_8 into UF_6 gas.

Operating reactors require the concentration of ^{235}U to be larger than the natural level. The concentration of ^{235}U can be increased through an enrichment process that utilized UF_6 as an input.

The final product of the enrichment is a UF_6 gas with enriched uranium.

The last step of the front-end processes is called the fabrication. The UF_6 gas is converted to a form of fuel (e.g. UO_2 for LWRs or UN for LFRs) that can be used in reactors, which is usually fuel pellet. The fuel pellets are fabricated and put into cylindrical cladding tubes. The fuel pins are assembled into fuel pin lattices referred to as fuel assemblies that are ready to be loaded in the reactor core.

After that, the fuel assemblies are loaded into the core of a power reactor and the reactor operation starts. The operation of the reactor generates revenue as it supplies the grid with electricity. At the end of the fuel cycle, three tasks will be performed. In the first, the first is the disposal of the spent fuel. The second is the dismantling of the reactor. The third is the decontamination of the plant site. The cost of these three tasks must be accounted for in the fuel cycle calculation.

A.3 Detailed Cost Calculations

A.3.1 Front End Costs

The Effective Full Power Days (EFPDs) of the reactor is calculated as;

$$\text{EFPD}\big[\text{days}\big] = \text{cycle\_length} \times 365.25 \tag{A.1}$$

where the cycle length is in years. The cycle total electric energy is calculated as;

$$\text{Cycle E. Energy}[\text{MW}_e.\text{hr}] = P_{\text{elec.}} \times \text{EFPD} \times 24 \tag{A.2}$$

where $P_{\text{elec.}}$ is the electric power output of the reactor in $[\text{MW}_e]$. The total mass of uranium in the core is calculated and used to calculate the $\left[\frac{\text{MWD}}{\text{MTU}}\right]$ energy from the fuel as;

$$\text{Cycle Specific Energy}\left[\frac{\text{MWD}}{\text{MTU}}\right] = \frac{P_{\text{thermal}} \times \text{EFPD}}{\text{Core uranium mass}} \tag{A.3}$$

The average discharge burnup in $\left[\frac{\text{GWD}}{\text{MTU}}\right]$ is calculated as;

$$\text{Average Burnup}\left[\frac{\text{GWD}}{\text{MTU}}\right] = \frac{\text{Cycle Specific Energy}}{1000} \tag{A.4}$$

The core investigated in this thesis is a fresh core at BOC. All the fuel inserted in the core is fresh and discharged at EOC (i.e. once-through fuel cycle). Thus the number of bundles is equal to the batch size.

The value function for feed, tails or product can be calculated according the to the following formula

$$V(\chi) = \big(2 \times E(\chi) - 1\big) \log\left(\frac{E(\chi)}{1 - E(\chi)}\right) \tag{A.5}$$

where E stands for the enrichment and χ represent the quantity of interest (i.e feed, tails or product). It should be noted that the enrichment is given as a fraction, not a percentage, (e.g. $E = 0.1$ if the enrichment is 10%). Then for each region in the core, the feed factor, tails factor and SWU factor are calculated as follows;

$$F_i = \text{Feed Factor}_i = \frac{E_{\text{Product},i} - E_{\text{Tail}}}{E_{\text{Feed}} - E_{\text{Tail}}} \tag{A.6}$$

$$T_i = \text{Tails Factor}_i = \frac{E_{\text{product},i} - E_{\text{feed}}}{E_{\text{feed}} - E_{\text{tail}}} \tag{A.7}$$

$$\text{SWU}_i = V(\text{Product}_i) + T_i \times V(\text{Tails}) - F_i \times V(\text{Feed}) \tag{A.8}$$

The subscript refers to the enrichment zone in the core (i.e. inner, middle or outer core in the case of WEC long-life LFR). The uranium mass flow into the SWU stage in the fuel cycle can be calculated as follows.

$$\begin{aligned} \text{SWU kgU}_i = &\text{U}_{\text{mass},i} \times \text{SWU}_i \times \\ &(1 + \text{Fabrication Loss}) \times (1 + \text{Enrichment Loss}) \end{aligned} \tag{A.9}$$

where $\text{U}_{\text{mass},i}$ is the mass of uranium in zone i. The uranium mass flow into the conversion process can be calculated as

$$\begin{aligned} \text{conversion kgU}_i = &\text{U}_{\text{mass},i} \times F_i \times \\ &(1 + \text{Fabrication Loss})(1 + \text{Conversion Loss}) \times \\ &(1 + \text{Enrichment Loss}) \end{aligned} \tag{A.10}$$

The base cost (BC) of the fabrication, SWU, conversion and ore can be calculated as

$$\text{Fabrication BC} = \text{Fabrication Cost} \times \sum_i \text{U}_{\text{mass},i} \tag{A.11}$$

$$\text{SWU BC} = \text{SWU Cost} \times \sum_i \text{SWU kgU}_i \tag{A.12}$$

$$\text{Conversion BC} = \text{Conversion Cost} \times \sum_i \text{Conversion kgU}_i \tag{A.13}$$

$$\text{ore BC} = \text{ore cost} \times c \times \sum_i \text{conversion kgU}_i \tag{A.14}$$

where the factor $c = 2.5998$ is the conversion from $\left[\text{kgU}\right]$ to [lb U_3O_8].

The price of a product of a process can change with time (e.g. in case of delays in purchases). To account for such uncertainties in ore, SWU, conversion and fabrication product costs, the escalation rate is used to adjust the value of the product of a process. First, the period from the time of planning the purchase until the process delivery is assumed. The following four variables are assumed.

- Fabrication TP $\left[\text{days}\right]$: Time from fab effective price to date of fab delivery.
- SWU TP $\left[\text{days}\right]$: Time from SWU effective price to date of SWU delivery.
- Conversion TP $\left[\text{days}\right]$: Time from conversion effective price to date of conversion delivery.
- Ore TP $\left[\text{days}\right]$: Time from ore effective price to date of ore delivery.

Then, using these time periods, the Escalation Factors (EFs) used to adjust the price of each purchase are calculated as follows

$$\text{Fabrication EF} = (1 + \text{Escalation Rate}/365.25)^{\text{Fabrication TP}} \tag{A.15}$$

$$\text{SWU EF} = (1 + \text{Escalation Rate}/365.25)^{\text{SWU TP}} \tag{A.16}$$

$$\text{Conversion EF} = (1 + \text{Escalation Rate}/365.25)^{\text{Conversion TP}} \tag{A.17}$$

$$\text{Ore EF} = (1 + \text{Escalation Rate}/365.25)^{\text{Ore TP}} \tag{A.18}$$

Then, these factors are applied to the base costs to calculate the Escalated Costs (EC) as

$$\text{Fabrication EC} = \text{Fabrication BC} \times \text{Fabrication EF} \tag{A.19}$$

$$\text{SWU EC} = \text{SWU\_BC} \times \text{SWU EF} \tag{A.20}$$

$$\text{Conversion EC} = \text{Conversion BC} \times \text{Conversion EF} \tag{A.21}$$

$$\text{Ore EC} = \text{Ore BC} \times \text{Ore EF} \tag{A.22}$$

The total front end cycle cost is calculated by summing up the escalated costs

$$\begin{aligned} \text{Front-End Cost} = &\text{Fabrication EC} \\ &+ \text{SWU EC} \\ &+ \text{Conversion EC} \\ &+ \text{Ore EC} \end{aligned} \tag{A.23}$$

Finally, it should be noted that the front-end cost of the fuel assemblies doesn't consider carrying costs. Considering the carrying costs will be presented in the following subsection

A.3.2 Carrying Costs

An important factor to be considered is the carrying charges. The carrying charge cost simply means accounting for the interest rate on the investment through the whole fuel cycle. The time period of the payment is considered to be from the purchase time until the end of the fuel cycle. This is the period during which the capital investment made on the fuel is payed back (The revenue of operating the core will pay for the fuel investment).

The carrying charge calculations are carried out on two stages. The first is the pre-operational carrying charges calculation and the second is the in-core carrying charges calculations. For the pre-operation carrying charges, the time period considered is from the time of a process (fabrication, SWU, conversion or ore extraction) delivery to the startup of cycle. The following Pre-Operational Time Periods (POTP) are assumed (based on experience, for example);

- Fabrication POTP $\left[\text{days}\right]$: The time from fabrication to initial burn.
- SWU POTP $\left[\text{days}\right]$: The time from SWU delivery to initial burn.
- Conversion POTP $\left[\text{days}\right]$: The time from Conversion delivery to initial burn.
- Ore POTP $\left[\text{days}\right]$: The time from ore delivery to initial burn.

These are used in calculating the pre-operation carrying charge factors (POCCF) as follows

$$\text{fabrication POCCF} = (1 + \text{Carrying Charge Rate}/365.25)^{\text{fabrication POTP}} - 1 \tag{A.24}$$

$$\text{SWU POCCF} = (1 + \text{Carrying Charge Rate}/365.26)^{\text{SWU POTP}} - 1 \tag{A.25}$$

$$\text{Conversion POCCF} = (1 + \text{Carrying Charge Rate}/365.25)^{\text{Conversion POTP}} - 1 \tag{A.26}$$

$$\text{Ore POCCF} = (1 + \text{Carrying Charge Rate}/365.25)^{\text{Ore POTP}} - 1 \tag{A.27}$$

These are used to calculate the Pre-Operational Carrying Charges Cost (POCCC) as follows.

$$\text{fabrication POCCC} = \text{fabrication EC} \times \text{fabrication POCCF} \tag{A.28}$$

$$\text{SWU POCCC} = \text{SWU EC} \times \text{SWU POCCF} \tag{A.29}$$

$$\text{Conversion POCCC} = \text{Conversion EC} \times \text{Conversion POCCF} \tag{A.30}$$

$$\text{Ore POCCC} = \text{Ore EC} \times \text{Ore POCCF} \tag{A.31}$$

The total POCCC is the sum of the previous four POCCCs;

$$\begin{aligned} \text{Total POCCC} = &\text{Fabrication POCCC} \\ &+ \text{SWU POCCC} \\ &+ \text{Conversion POCCC} \\ &+ \text{Ore POCCC} \end{aligned} \tag{A.32}$$

To calculate the in-core carrying cost, the cycle Carrying Charge Factor (CCF) is calculated as follows

$$\text{Cycle CCF} = (1 + \text{Carrying Charge Rate}/12)^{\text{Cycle Length}} - 1 \tag{A.33}$$

Then, the In-Core Carrying Charge (ICCC) is calculated based on the linear energy allocation model as

$$\text{ICCC} = 0.5 \times \text{Cycle CCF} \tag{A.34}$$

The in-core carrying charge cost is calculated as follows;

$$\text{ICCC Cost} = \text{ICCC} \times (\text{Front End Cost} + \text{Total POCCC}) \tag{A.35}$$

The property taxes are calculated as follows

$$\begin{aligned} \text{Property Tax} = &0.5 \times \text{Property Tax Rate} \times (\text{Cycle Length}/12) \\ &\times \text{Front-End Cost} \end{aligned} \tag{A.36}$$

where the cycle length is in months. The dismantling and disposal (D&D) costs are calculated as follows;

$$\text{D\&D} = \text{D\&D rate} \times \text{Cycle Length} \tag{A.37}$$

The disposal cost is calculates as follow;

$$\text{Disposal} = \text{Disposal Rate} \times \text{Cycle E. Energy} \tag{A.38}$$

The total fuel cycle cost is calculated as follows;

$$\begin{aligned}\text{Total Fuel Cycle Cost} =& \text{Total Front End} + \text{Total POCCC} \\ &+ \text{ICCC Cost} + \text{Property Tax} \\ &+ \text{D\&D} + \text{Disposal}\end{aligned} \tag{A.39}$$

A.4 Calculating The LCOE

To calculate the LCOE, total cost of the fuel cycle is spread over the operation time of the reactor in an attempt to find the cost of electricity that makes the project breakeven. The levelized cost of electricity is calculated as follows;

$$\text{LCOE} = \frac{\text{Total Fuel Cycle Cost}}{\text{Cycle E. Energy}}$$

A.5 Example

In this section, an example of the fuel cycle economic calculations will be given. The case of the WEC long-life core LFR will be used. The masses calculated for the design will be used. These masses are presented in Table A.1. The assumptions and values were presented in Table 3.1 and Table 3.2.

Table A.1 Beginning of Cycle Heavy Metal Masses

Region	Mass of U^{235} [kg]	Mass of U^{238} [kg]	Enrichment [%]
Inner Core	2217.90	19315.18	10.3
Middle Core	2315.73	17309.15	11.8
Outer Core	5190.71	32423.13	13.8

Total KgU = 78771.8

The thermal and electrical power of the core is 950 [$MW_t\,h$] and 456 [MW_e]. According to [Kim19], the cycle length is 25 [years] (i.e. 300 [months]). The number of effective full power days is calculated as

$$\text{EFPD} = 9131.25\,[\text{days}] \tag{A.40}$$

The cycle total electric energy is

$$\text{Cycle E. Energy} = 99932400\,[\text{MW}_e.\text{hr}] \tag{A.41}$$

The reactor average burnup can be calculated as

$$\begin{aligned}\text{Average Burnup} &= \frac{P_{\text{Rx}} \times \text{cycle length in days}}{\text{uranium Mass}} \\ &= \frac{950 \times 25 \times 365.25}{78693} \\ &= 107.93\left[\frac{\text{GWd}}{\text{MTHM}}\right]\end{aligned} \tag{A.42}$$

The value function of feed is

$$V(\text{feed}) = 4.87038 \tag{A.43}$$

The enrichment, feed and tails enrichment were presented in Table 3.2. The value function of tails is

$$V(\text{tails}) = 5.95902 \tag{A.44}$$

The value function of product is calculated for each enrichment zone separately as

$$V(\text{inner core}) = 1.71848 \tag{A.45}$$

$$V(\text{middle core}) = 1.53679 \tag{A.46}$$

$$V(\text{outer core}) = 1.32637 \tag{A.47}$$

The feed factor for each region in the core is calculated as

$$\begin{aligned}\text{Feed Factor of inner core} &= 21.84783 \\ \text{Feed Factor of middle core} &= 25.10870 \\ \text{Feed Factor of outer core} &= 29.45652\end{aligned} \tag{A.48}$$

The tails factor for the three regions can be calculated as

$$\begin{aligned}\text{Tails factor for inner core} &= 20.84783 \\ \text{Tails factor for middle core} &= 24.10870 \\ \text{Tails factor for outer core} &= 28.45652\end{aligned} \tag{A.49}$$

The SWU factor for the three regions is

$$\begin{aligned} \text{SWU factor for inner core} &= 19.54381 \\ \text{SWU factor for middle core} &= 22.91203 \\ \text{SWU factor for outer core} &= 27.43481 \end{aligned} \tag{A.50}$$

The mass flow (in kgU) into the SWU process for each region in the core is as follows

$$\begin{aligned} \text{SWU kgU inner core} &= 423,365\big[\text{kgU}\big] \\ \text{SWU kgU middle core} &= 452,346\big[\text{kgU}\big] \\ \text{SWU kgU outer core} &= 1,038,125\big[\text{kgU}\big] \end{aligned} \tag{A.51}$$

The total SWU kgU is the simply sum SWU kgU of inner and middle and outer core regions

$$\text{Total SWU kgU} = 1,913,837 \tag{A.52}$$

The conversion process mass input (kgU) for the three regions of the cores is as follows

$$\begin{aligned} \text{Conversion kgU inner core} &= 475,642\big[\text{kgU}\big] \\ \text{Conversion kgU middle core} &= 498,193\big[\text{kgU}\big] \\ \text{Conversion kgU outer core} &= 1,120,199\big[\text{kgU}\big] \end{aligned} \tag{A.53}$$

The total conversion kgU is the sum of the conversion kgU required for inner, middle and outer core region fuels

$$\text{Total conversion kgU} = 2,094,035 \tag{A.54}$$

The U_3O_8 mass in [lb] for each region of the core is as follows

$$\begin{aligned} \text{[lb] } U_3O_8 \text{ for the inner core} &= 1,236,586\,[\text{lb } U_3O_8] \\ \text{[lb] } U_3O_8 \text{ for the middle core} &= 1,295,213\,[\text{lb } U_3O_8] \\ \text{[lb] } U_3O_8 \text{ for the outer core} &= 2,912,319\,[\text{lb } U_3O_8] \end{aligned} \tag{A.55}$$

The total U_3O_8 mass required will be the sum of the U_3O_8 mass required masses for the inner, middle and outer core regions.

$$\text{Total [lb] } U_3O_8 = 5,444,120 \tag{A.56}$$

Using the values presented in Table 3.1 the cost of the components of the front end of the fuel

cycle is a (i.e. Base Cost).

$$\begin{aligned} \text{Fabrication BC} &= 39,385,917\,[\$] \\ \text{SWU BC} &= 133,968,641\,[\$] \\ \text{Conversion BC} &= 20,940,354\,[\$] \\ \text{Ore BC} &= 217,764,802\,[\$] \end{aligned} \tag{A.57}$$

Before calculating the front end, the base costs will be escalated first. The time periods based on which the escalation was calculated are provided in Table A.2. These are typical values used in fuel cycle analysis.

Table A.2 Escalation Time Periods

parameter	Time period [days]
Fabrication	610
SWU	550
Conversion	490
Ore	490

The escalation factors for the fabrication, SWU, conversion and ore are presented in Table A.3.

Table A.3 Escalation Factors

Parameter	Escalation Factors
Fabrication EF	1.087
SWU EF	1
Conversion EF	1
Ore EF	1

Applying these factors to the base costs and summing the escalated costs together, we get the total front-end cost.

$$\text{Front-end Costs} = 415,492,039\,[\$] \tag{A.58}$$

To calculate the POCCR, the assumed POTP are as follows

$$\begin{aligned} \text{Fabrication POTP} &= 120\left[\text{days}\right] \\ \text{SWU POTP} &= 180\left[\text{days}\right] \\ \text{Conversion POTP} &= 240\left[\text{days}\right] \\ \text{Ore POTP} &= 240\left[\text{days}\right] \end{aligned} \tag{A.59}$$

Based on these values, the POCCR will be as in Table A.4.

Table A.4 Pre-Operational Carrying Charge Rates

Parameter	POCCR
Fabrication	2.0%
SWU	3.0%
Conversion	4.0%
Ore	4.0%

Using the escalated costs and the pre-operational carrying charges, the pre-operational carrying charge costs are calculated

$$\begin{aligned} \text{Fabrication POCCC} &= 852,949\,[\$] \\ \text{SWU POCCC} &= 4,022,896\,[\$] \\ \text{Conversion POCCC} &= 842,582\,[\$] \\ \text{Ore POCCC} &= 8,762,257\,[\$] \end{aligned} \tag{A.60}$$

The total POCCC is the summation of the previous four POCCC,

$$\text{Total POCCC} = 14,480,684\,[\$] \tag{A.61}$$

The cycle CCF is

$$\text{Cycle CCF} = 0.648 \tag{A.62}$$

The ICCC rate is

$$\text{ICCC Rate} = 0.324 \tag{A.63}$$

The ICCC Cost is

$$\text{ICCC Cost} = 139,318,732\,[\$] \tag{A.64}$$

Finally the D&D and disposal costs are

$$\begin{aligned} \text{D\&D Total Cost} &= 24,748,200\,[\$] \\ \text{Disposal} &= 99,932,400\,[\$] \end{aligned} \tag{A.65}$$

the value of D&D value can be found in Table 3.2. By summing the front-end, D&D, disposal and carrying charges costs, the total fuel cycle cost is

$$\text{Total Fuel Cycle Cost} = 693,972,055\,[\$] \tag{A.66}$$

Finally, the LCOE is

$$\text{LCOE} = 6.94\left[\frac{\$}{\text{MW}_e\text{hr}}\right] \tag{A.67}$$

This value of LCOE represents the price of the MW_ehr that results in a break even profit from operating the cycle. In [Kim19], the calculated LCOE was 7.5 $\left[\frac{\$}{\text{MW}_e\text{hr}}\right]$. The difference could be related to utilizing different methodologies. It should be noted that the authors of [Kim19] did not include details about their methodology for calculating the fuel cycle cost. The break down of the costs is presented in Table A.5. The contribution of the carrying charges is 22.2 [%]

Table A.5 Breakdown of Costs

Parameter	Cost [$]	Contribution to cost [%]
Ore	217,764,802	31.4
Conversion	20,940,354	3.0
SWU	133,968,641	19.3
Fabrication	42,818,243	6.2
Pre-Operational carrying costs	14,480,684	2.1
In-Core carrying costs	139,318,732	20.1
D&D	24,748,200	3.6
Disposal cost	99,932,400	14.4

APPENDIX

B

INSIGHTS FOR APPLYING DOM

B.1 Introduction

DOM has been presented in Chapter 3 and tested in Chapter 4. Using DOM, a gain of 2.56 [%] has been achieved on LCOE. In this appendix, the goal is to present a run of the Python program that applies DOM to optimize the WEC long-life core LFR. This case was run with the domain of search space presented Table 4.8.

B.2 Summary of the Run

The purpose of this run is to provide some illustration of the process of using DOM. Two thousand cases were requested from the Python LHS module. Table B.1 presents some statistics. The cases that pass the thermal hydraulic test and start supercritical are presented in Table B.2. These cases were analyzed and their LCOE was calculated. The samples that have a LCOE smaller than that of the original design are written in red.

Table B.1 Statistics of the run

Parameter	No. Cases
Total cases	2000
Successful cases	1022
Critical cases[a]	231

[a] critical cases are those with BOC $k_{\text{eff}} > 1.00308$

Table B.2 Successful samples and their calculated LCOE

R_{pin}	P_{pin}	H_{pin}	N_{rings}	E_{ic}	E_{mc}	E_{oc}	LCOE
0.6538	1.5175	235.1529	6.0000	8.5103	11.1227	16.2670	17.5313
0.6575	1.5474	230.7773	6.0000	8.0244	11.2366	16.6390	15.0457
0.6279	1.5457	234.1729	6.0000	7.5019	11.9919	16.4062	39.2839
0.6158	1.4566	241.2084	6.0000	7.5043	11.9254	16.4703	118.8510
0.6502	1.5337	220.5415	6.0000	7.2504	11.7583	16.8913	17.8346
0.6649	1.5294	220.0893	6.0000	9.8829	11.4133	14.6039	8.8414
0.8426	1.9209	244.4422	5.0000	9.3744	11.5246	15.0010	6.9733
0.6859	1.5784	215.2215	6.0000	7.8885	11.7822	16.2293	10.4876
0.7825	1.8286	228.4679	5.0000	9.0085	11.0038	15.8876	50.4366
0.6592	1.5260	240.3227	6.0000	9.9250	11.5049	14.4700	8.2701
0.8365	1.9037	212.2272	5.0000	9.5106	11.6259	14.7635	7.0191
0.7855	1.8838	229.3170	5.0000	8.7923	11.5918	15.5159	35.5557
0.6238	1.4880	220.2349	6.0000	7.6670	11.0800	17.1530	50.3999
0.7818	1.9226	216.6295	5.0000	7.7880	11.0756	17.0364	24.4603
0.6457	1.5291	246.6515	6.0000	10.9097	11.7849	13.2054	9.2593
0.6369	1.4855	231.1884	6.0000	8.1899	11.8369	15.8733	54.5483
0.8098	1.9192	230.4713	5.0000	10.7354	11.1512	14.0134	7.8473
0.6530	1.5566	230.3819	6.0000	10.7396	11.0763	14.0841	9.0899
0.8394	1.9145	217.2907	5.0000	10.7158	11.9457	13.2386	7.0488
0.6191	1.5847	229.1055	6.0000	7.4840	11.9250	16.4911	290.8515
0.8160	1.8697	214.4063	5.0000	7.6732	11.7079	16.5189	13.9416
0.7569	1.8622	225.3478	5.0000	7.6392	11.8483	16.4125	223.0484
0.6573	1.5492	213.0853	6.0000	9.6358	11.1129	15.1513	68.2915
0.8105	1.8967	247.0561	5.0000	8.1412	11.9677	15.7912	11.5431
0.6553	1.5748	220.3066	6.0000	8.8881	11.4747	15.5372	27.0340
0.6482	1.5684	210.7290	6.0000	8.7056	11.8100	15.3845	78.1066
0.7788	1.8977	241.7948	5.0000	8.0863	11.9080	15.9057	30.6109
0.6797	1.5596	240.9040	6.0000	7.3655	11.3577	17.1768	10.3601
0.6360	1.4920	223.6814	6.0000	8.3010	11.1233	16.4757	48.1196
0.6922	1.5778	221.9635	6.0000	8.7108	11.4612	15.7280	7.2032
0.6918	1.5805	244.3993	6.0000	10.3091	11.1653	14.4256	6.9973
0.8117	1.9326	219.3479	5.0000	8.7975	11.2950	15.8076	14.4042
0.7904	1.9088	224.6265	5.0000	9.0943	11.2757	15.5301	31.2889
0.6559	1.5521	235.3505	6.0000	7.9341	11.4481	16.5178	16.7206
0.6679	1.5551	232.7529	6.0000	9.0281	11.7957	15.0762	9.4076
0.6516	1.5760	227.8945	6.0000	7.8919	11.5901	16.4180	19.4424

Continued on next page

Table B.2 – *Continued from previous page*

R_{pin}	P_{pin}	H_{pin}	N_{rings}	E_{ic}	E_{mc}	E_{oc}	LCOE
0.7994	1.8941	249.7748	5.0000	10.7478	11.8633	13.2889	8.4229
0.6692	1.5612	213.4710	6.0000	9.0783	11.2187	15.6029	9.8122
0.7667	1.9205	221.3005	5.0000	7.3382	11.0729	17.4889	30.0109
0.6293	1.5500	211.9675	6.0000	7.2353	11.3535	17.3112	36.5583
0.6723	1.5688	218.9531	6.0000	7.4379	11.3927	17.0694	12.3588
0.6460	1.5158	228.8518	6.0000	9.0994	11.3262	15.4744	107.9464
0.6391	1.5153	232.5208	6.0000	7.6787	11.6174	16.6039	24.8340
0.7001	1.5841	217.2324	6.0000	7.8361	11.8870	16.1770	8.2254
0.8226	1.8922	234.0658	5.0000	10.9715	11.2129	13.7156	7.3938
0.6142	1.5788	225.8801	6.0000	7.3757	11.1642	17.3601	86.5816
0.7692	1.9088	243.2588	5.0000	7.3314	11.5978	16.9708	28.5774
0.6501	1.5485	242.6235	6.0000	8.1166	11.5155	16.2678	18.4557
0.6827	1.5656	222.1544	6.0000	9.4200	11.4204	15.0597	7.3600
0.7604	1.7946	221.2789	5.0000	7.6102	11.3159	16.9739	60.5038
0.8361	1.9236	247.9127	5.0000	9.8270	11.2953	14.7777	7.0499
0.8296	1.9259	233.2329	5.0000	9.4684	11.9731	14.4585	7.2119
0.6839	1.5805	246.5177	6.0000	10.4516	11.5669	13.8815	7.2849
0.6341	1.4869	238.8612	6.0000	7.6070	11.9845	16.3085	32.5380
0.6270	1.5183	225.6428	6.0000	7.9676	11.2843	16.6482	68.9763
0.6677	1.5709	221.5009	6.0000	7.4740	11.0986	17.3274	13.5162
0.8492	1.9488	233.9652	5.0000	9.1049	11.4627	15.3324	6.9281
0.6489	1.5071	224.6792	6.0000	8.4121	11.6748	15.8130	28.4639
0.7890	1.9258	245.2594	5.0000	8.0321	11.3446	16.5233	19.4300
0.8018	1.9091	217.6728	5.0000	8.0030	11.3877	16.5093	17.0488
0.8003	1.8786	226.2768	5.0000	10.0429	11.8054	14.0517	9.1069
0.6641	1.5629	244.6157	6.0000	7.4075	11.7531	16.7393	13.2950
0.7589	1.8626	214.9972	5.0000	7.3455	11.5956	16.9590	59.6947
0.6342	1.4928	233.7385	6.0000	8.2907	11.2429	16.3664	39.0520
0.7794	1.9012	229.5842	5.0000	8.5155	11.2252	16.1592	44.8820
0.8272	1.9177	211.5543	5.0000	8.7479	11.4759	15.6762	10.0566
0.7452	1.8899	237.5953	5.0000	7.4408	11.5775	16.8816	162.9189
0.6769	1.5926	245.4651	6.0000	8.8066	11.0488	16.0446	7.9957
0.7915	1.8931	249.0841	5.0000	9.1630	11.2536	15.4834	20.5062
0.6116	1.4431	240.4948	6.0000	7.6125	11.6995	16.5880	1076.5513
0.7712	1.8615	234.4677	5.0000	7.5483	11.7461	16.6057	35.2241
0.6737	1.5614	243.6408	6.0000	10.9995	11.2574	13.6431	7.4668

Continued on next page

Table B.2 – *Continued from previous page*

R_{pin}	P_{pin}	H_{pin}	N_{rings}	E_{ic}	E_{mc}	E_{oc}	LCOE
0.6656	1.5827	225.3393	6.0000	8.1895	11.4583	16.2522	13.7805
0.8283	1.9188	213.2343	5.0000	10.3059	11.3372	14.2569	7.5352
0.8108	1.8785	219.3926	5.0000	10.7139	11.3315	13.8546	8.3416
0.6397	1.5373	211.4534	6.0000	7.7200	11.3036	16.8764	33.3240
0.8068	1.8981	233.5724	5.0000	10.6839	11.7440	13.4721	8.0243
0.6102	1.5783	247.6598	6.0000	7.5920	11.2847	17.0233	300.7631
0.8063	1.9181	231.7463	5.0000	8.1221	11.9084	15.8695	14.7860
0.7615	1.8800	214.5419	5.0000	7.3497	11.1708	17.3795	45.0059
0.6658	1.5544	230.8108	6.0000	10.2658	11.8417	13.7925	8.0319
0.7966	1.8905	231.0469	5.0000	7.7264	11.3250	16.8485	15.8422
0.6554	1.5738	247.3290	6.0000	10.0581	11.1589	14.6830	8.4060
0.6920	1.5715	212.4260	6.0000	10.2725	11.5187	14.1088	7.1127
0.6563	1.5295	216.1735	6.0000	9.2039	11.0361	15.6600	28.1483
0.6751	1.5820	221.0972	6.0000	10.6451	11.0030	14.2520	7.6692
0.7916	1.8671	248.2984	5.0000	9.1195	11.7600	15.0205	13.7038
0.8136	1.8990	238.8962	5.0000	9.1068	11.3369	15.4563	7.9567
0.6523	1.5633	241.7489	6.0000	7.6404	11.2483	17.0113	15.2507
0.6625	1.5478	220.0657	6.0000	8.3224	11.6033	15.9743	14.3329
0.7928	1.9345	234.6408	5.0000	9.6751	11.4489	14.7760	13.3381
0.7871	1.9287	240.5662	5.0000	7.7048	11.4898	16.7055	19.2015
0.6597	1.5222	220.7504	6.0000	7.3410	11.2516	17.3073	14.7645
0.6579	1.5517	233.3428	6.0000	10.8303	11.8076	13.2621	8.5072
0.8603	1.9430	234.1189	5.0000	7.3444	11.1855	17.3702	8.4438
0.6945	1.5908	215.6873	6.0000	8.9149	11.6163	15.3688	7.0920
0.6904	1.5803	214.5280	6.0000	10.3118	11.6987	13.8895	7.1137
0.6346	1.5214	245.6070	6.0000	8.3503	11.3222	16.2275	34.2264
0.8186	1.9188	215.1591	5.0000	8.7955	11.7351	15.3694	9.3709
0.6542	1.5667	239.3807	6.0000	8.7550	11.9601	15.1850	16.1090
0.7937	1.8586	222.1705	5.0000	9.5314	11.5615	14.8071	262.9717
0.7969	1.8765	220.1861	5.0000	8.2112	11.1323	16.5565	17.8563
0.6363	1.5851	245.3289	6.0000	8.5876	11.1252	16.1873	42.6356
0.6126	1.4554	249.8342	6.0000	7.7152	11.2163	16.9685	111.8711
0.6616	1.5767	244.8619	6.0000	8.9345	11.5658	15.3997	11.5643
0.8244	1.9078	238.2821	5.0000	7.7483	11.9022	16.2495	10.8066
0.7730	1.8983	247.8404	5.0000	8.5891	11.7201	15.5908	58.9517
0.6620	1.5789	216.1260	6.0000	7.6380	11.3050	16.9570	15.5070

Continued on next page

Table B.2 – *Continued from previous page*

R_{pin}	P_{pin}	H_{pin}	N_{rings}	E_{ic}	E_{mc}	E_{oc}	LCOE
0.6505	1.5084	248.9629	6.0000	8.6720	11.6294	15.5986	16.5698
0.7977	1.8470	211.0066	5.0000	9.3608	11.9969	14.5423	61.9700
0.8000	1.9019	214.2482	5.0000	7.7905	11.4601	16.6495	19.0483
0.6590	1.5554	212.2707	6.0000	7.8698	11.7939	16.2362	18.5316
0.6584	1.5622	240.5814	6.0000	10.4904	11.5845	13.8251	8.1183
0.8022	1.8658	238.3079	5.0000	9.4790	11.1158	15.3052	8.7056
0.8041	1.8939	226.0663	5.0000	9.6781	11.2707	14.9512	8.9374
0.8263	1.9260	212.7682	5.0000	9.8926	11.7496	14.2578	7.4269
0.6558	1.5284	225.1981	6.0000	10.4169	11.1269	14.3562	8.9429
0.8175	1.9271	215.5595	5.0000	10.0787	11.7157	14.1056	8.0571
0.6475	1.5555	235.3809	6.0000	8.5945	11.2941	16.0114	24.3450
0.7967	1.8960	240.0089	5.0000	8.0786	11.4711	16.3504	15.8256
0.6480	1.5277	249.5113	6.0000	9.3799	11.5410	14.9791	14.3529
0.6233	1.5136	223.1957	6.0000	7.3475	11.0057	17.5468	35.3579
0.7949	1.8377	229.0837	5.0000	7.6235	11.8717	16.4047	18.0916
0.6380	1.5437	229.7168	6.0000	8.4313	11.3966	16.0720	57.3931
0.6185	1.5326	247.4337	6.0000	7.3608	11.0921	17.4471	34.6845
0.8273	1.9384	227.0974	5.0000	7.3838	11.6974	16.8188	11.2511
0.7660	1.8280	244.9870	5.0000	8.1769	11.8792	15.8439	83.0797
0.6415	1.5400	236.1769	6.0000	7.3303	11.5858	16.9839	19.7769
0.6390	1.5083	225.1394	6.0000	7.9625	11.2783	16.6592	29.7853
0.8378	1.9081	233.5496	5.0000	9.7547	11.8936	14.2517	6.9570
0.6173	1.4917	211.6894	6.0000	7.3696	11.0279	17.5025	65.0149
0.7893	1.8522	231.3096	5.0000	7.5873	11.3064	17.0062	18.3947
0.6589	1.5173	233.6854	6.0000	10.5682	11.8623	13.4696	8.3977
0.8012	1.8711	246.0430	5.0000	8.2841	11.2276	16.3883	15.1469
0.7883	1.8510	246.3922	5.0000	7.7634	11.2074	16.9293	18.4798
0.7940	1.9133	239.7809	5.0000	9.4355	11.4083	15.0562	21.9389
0.7925	1.9250	219.9598	5.0000	7.7624	11.5204	16.6173	20.2135
0.7786	1.8472	221.2499	5.0000	8.2180	11.7073	15.9747	71.2248
0.6435	1.5336	247.9639	6.0000	8.8663	11.4904	15.5433	25.9686
0.6321	1.5859	246.4420	6.0000	7.9795	11.3178	16.6027	35.1759
0.8005	1.8964	217.4338	5.0000	10.9257	11.0074	13.9669	9.0642
0.6429	1.5849	236.0437	6.0000	8.4340	11.2960	16.1699	27.9255
0.7509	1.7838	225.2887	5.0000	7.2983	11.9612	16.6406	409.2193
0.7918	1.8754	243.6156	5.0000	9.5583	11.6991	14.6426	10.1170

Continued on next page

Table B.2 – *Continued from previous page*

R_{pin}	P_{pin}	H_{pin}	N_{rings}	E_{ic}	E_{mc}	E_{oc}	LCOE
0.6454	1.5543	220.5218	6.0000	8.8228	11.3057	15.7715	49.2012
0.7663	1.9405	240.9676	5.0000	7.8482	11.6306	16.4213	55.9057
0.8145	1.9160	212.0003	5.0000	7.6843	11.8129	16.4028	14.6427
0.6495	1.5768	228.9208	6.0000	9.5065	11.2570	15.1365	55.5299
0.8242	1.8854	243.7906	5.0000	7.2633	11.9475	16.6892	10.6797
0.7649	1.8168	237.7591	5.0000	7.9059	11.2151	16.7790	52.3041
0.8014	1.8974	249.1737	5.0000	10.1778	11.2032	14.5190	8.0404
0.7818	1.9027	224.0715	5.0000	8.5471	11.6884	15.6645	114.0591
0.6760	1.5750	243.5464	6.0000	9.4419	11.3612	15.0969	7.6012
0.7765	1.8349	224.4600	5.0000	8.4781	11.6470	15.7748	134.6581
0.8076	1.8994	212.5160	5.0000	9.6934	11.9281	14.2785	10.9222
0.6497	1.5679	239.5162	6.0000	8.7824	11.6543	15.4633	20.6331
0.8115	1.9251	221.5828	5.0000	7.4896	11.7252	16.6852	13.5501
0.8081	1.8858	246.7616	5.0000	10.4650	11.9770	13.4581	7.9155
0.7519	1.8644	241.5340	5.0000	7.8962	11.2433	16.7605	164.2386
0.7997	1.9051	233.7862	5.0000	10.7743	11.3618	13.7639	8.4749
0.6628	1.5679	226.8846	6.0000	10.8202	11.3333	13.7465	8.4569
0.6307	1.5775	241.7360	6.0000	8.1196	11.7835	15.9968	65.1643
0.6400	1.5172	223.2727	6.0000	7.8530	11.7954	16.2515	28.3017
0.7556	1.8456	245.7123	5.0000	7.9366	11.8636	16.0998	578.6664
0.6693	1.5714	212.0361	6.0000	9.3847	11.6253	14.8900	8.8852
0.6349	1.4909	222.7168	6.0000	7.7919	11.3081	16.7999	34.4816
0.6323	1.5189	218.3825	6.0000	7.2261	11.9316	16.7423	31.1035
0.7672	1.9185	219.4350	5.0000	8.0455	11.6024	16.2522	424.9301
0.8185	1.9469	219.5842	5.0000	10.2620	11.6339	14.0041	7.9341
0.8017	1.9321	236.1062	5.0000	7.5313	11.6780	16.6907	14.5210
0.8333	1.9042	219.9695	5.0000	8.8462	11.3890	15.6647	7.6809
0.8060	1.8770	243.8599	5.0000	8.9738	11.7392	15.1870	9.1850
0.8294	1.9072	222.3585	5.0000	9.5472	11.9888	14.3640	7.2470
0.7899	1.8331	215.0224	5.0000	8.3880	11.9683	15.5437	32.8069
0.7679	1.8379	245.4350	5.0000	8.3737	11.5939	15.9324	82.7412
0.6720	1.5667	212.9468	6.0000	9.5813	11.2616	15.0571	8.2204
0.8209	1.9028	210.4225	5.0000	9.7438	11.8257	14.3305	8.1710
0.6709	1.5863	227.5623	6.0000	10.8957	11.1478	13.8565	7.7784
0.8061	1.8895	223.1146	5.0000	9.9968	11.4887	14.4145	8.6740
0.8218	1.9241	216.2958	5.0000	10.9663	11.7944	13.1393	7.6671

Continued on next page

Table B.2 – *Continued from previous page*

R_{pin}	P_{pin}	H_{pin}	N_{rings}	E_{ic}	E_{mc}	E_{oc}	LCOE
0.7540	1.7991	229.2969	5.0000	7.8291	11.0604	17.0106	132.7812
0.6715	1.5620	222.2360	6.0000	10.1912	11.2996	14.4092	7.7337
0.6939	1.5763	215.4893	6.0000	7.3813	11.9290	16.5896	9.7829
0.8320	1.9193	245.8280	5.0000	7.2954	11.6103	16.9943	9.8092
0.7688	1.8158	230.2224	5.0000	7.5657	11.6105	16.7238	38.3034
0.7701	1.9101	243.9872	5.0000	7.6162	11.7147	16.5691	30.4410
0.6789	1.5650	238.2759	6.0000	7.5810	11.4123	16.9067	10.1973
0.6190	1.5007	245.9215	6.0000	7.4983	11.1000	17.3017	43.8851
0.7839	1.8722	233.6433	5.0000	8.1114	11.6662	16.1225	26.7326
0.7696	1.8553	218.1234	5.0000	7.9584	11.2623	16.6793	54.2555
0.6623	1.5636	244.1217	6.0000	7.9493	11.1985	16.7522	13.6137
0.7816	1.9328	222.9073	5.0000	8.0733	11.9229	15.9038	41.5452
0.6406	1.5309	228.9581	6.0000	8.1437	11.8179	15.9384	35.0553
0.6370	1.4962	221.7761	6.0000	8.1873	11.1197	16.5929	43.2340
0.6637	1.5419	225.1442	6.0000	8.8904	11.2099	15.7997	12.0164
0.6736	1.5901	226.1729	6.0000	8.6136	11.5056	15.7807	10.5841
0.6825	1.5729	216.9890	6.0000	7.7842	11.7910	16.3248	10.7666
0.7867	1.9267	239.5363	5.0000	7.9038	11.0023	16.9938	20.6823
0.6535	1.5667	226.4950	6.0000	9.2055	11.4936	15.2010	32.8948
0.7653	1.8656	217.5531	5.0000	7.3771	11.0868	17.4361	37.9229
0.7053	1.5924	228.3725	6.0000	10.5639	11.8356	13.5005	6.8406
0.6845	1.5750	215.9489	6.0000	9.6155	11.2966	14.9879	7.3500
0.6957	1.5770	245.4563	6.0000	8.3218	11.8187	15.7595	6.9746
0.8096	1.8816	221.4546	5.0000	8.5588	11.4233	15.9179	14.2170
0.6007	1.4692	239.8891	6.0000	7.2388	11.0426	17.6186	345.4087
0.6480	1.5690	231.6096	6.0000	8.2674	11.1949	16.4376	20.2583
0.7985	1.8658	230.0168	5.0000	10.3072	11.5142	14.0786	8.6343
0.7980	1.8691	228.7505	5.0000	7.9432	11.3963	16.5605	17.5094
0.8438	1.9287	243.1035	5.0000	7.9708	11.5434	16.3858	7.2376
0.6721	1.5586	232.2899	6.0000	8.1260	11.1711	16.6029	11.9408
0.8058	1.8789	228.3590	5.0000	9.2627	11.5790	15.0583	9.1609
0.6716	1.5773	246.3531	6.0000	9.4111	11.2016	15.2873	7.7093
0.7457	1.8377	230.0306	5.0000	7.4928	11.5223	16.8850	401.6101
0.6659	1.5566	210.0616	6.0000	7.7018	11.3385	16.8597	14.1229
0.6668	1.5810	217.4425	6.0000	8.1592	11.6945	16.0463	13.7165
0.6264	1.4992	221.4767	6.0000	7.7951	11.8773	16.2276	396.5248

Continued on next page

Table B.2 – *Continued from previous page*

R_{pin}	P_{pin}	H_{pin}	N_{rings}	E_{ic}	E_{mc}	E_{oc}	LCOE
0.6888	1.5876	210.0360	6.0000	9.7044	11.9893	14.2063	7.2299
0.6450	1.5691	227.0787	6.0000	8.0100	11.4415	16.4485	25.1728
0.6345	1.5418	210.0872	6.0000	8.0012	11.3006	16.5982	52.8271
0.6608	1.5567	221.1514	6.0000	10.1108	11.4208	14.3684	8.7097
0.8311	1.9181	210.7532	5.0000	8.5636	11.8529	15.4835	8.5469
0.6705	1.5673	238.8447	6.0000	9.1814	11.4049	15.3137	7.7522
0.7807	1.9290	217.1578	5.0000	7.6347	11.8153	16.4499	32.2306
0.7506	1.8595	230.3446	5.0000	7.5168	11.4259	16.9572	89.1333
0.7781	1.9010	234.0809	5.0000	7.2470	11.5030	17.1500	21.4377
0.6701	1.5907	210.3118	6.0000	10.7856	11.0203	14.0941	8.2038
0.8025	1.8909	214.4585	5.0000	7.6649	11.5693	16.6658	16.3506
0.6427	1.5762	214.9533	6.0000	8.3996	11.2860	16.2145	41.1046
0.6207	1.4698	225.0545	6.0000	7.9212	11.1699	16.8089	131.5665
0.6302	1.5727	227.6812	6.0000	8.2369	11.0862	16.5769	66.4055
0.6312	1.5181	239.9189	6.0000	7.6989	11.1873	17.0138	30.4923